CHAPTER 4:
CHROMOSPHERIC EXPLOSIONS

by

G.A. Doschek[a], S.K. Antiochos[b], E. Antonucci, C.-C. Cheng, J.L. Culhane, G.H. Fisher, C. Jordan, J.W. Leibacher, P. MacNeice, R.W.P. McWhirter, R.L. Moore, D.M. Rabin, D.M. Rust, and R.A. Shine

[a]Chapter editor and Team leader

[b]Underlined team members were responsible for substantial written contributions for the chapter.

4.1 INTRODUCTION

The subject of investigation for Team D is rather loosely called "Chromospheric Explosions". Chromospheric explosions includes the response and relationship of the flare chromosphere and transition region to the hot coronal loops that reach temperatures of about 10^7K and higher. It also includes flare related phenomena such as surges and sprays. In particular, the team decided to focus on some of those aspects of coronal and chromospheric phenomena that are newly-observed by the complement of instruments flown on SMM and other recent spacecraft such as P78-1 and Hinotori.

During the first two Workshops, it became apparent that the interpretation of some of the newly obtained X-ray spectra is quite controversial. In addition, there are differing opinions concerning theoretical aspects of flares, such as the role of electron beams versus thermal conduction in heating the chromosphere. The team therefore decided to focus on three controversial issues as Workshop projects, and to try to improve our understanding of these issues by presenting the work in terms of debates between two sub-teams. This was a reasonable approach because the team was not very large. An issue to be debated was written down precisely, and the team divided itself into two camps, pro and con. Each team member picked the position that at the time seemed most reasonable to that member. As the work progressed, some team members decided that the position of the other sub-team was stronger, but nevertheless remained on their initially chosen team and took the position of a devil's advocate. Thus, in this chapter individual members of the sub-teams are not identified, since their current feelings about the debated issues may not reflect their positions during the debates.

Each sub-team had a sub-team coordinator whose responsibility was to collect material from sub-team members, organize it into a coherent argument, and then present the argument as part of a debate during the final Workshop. The sub-team coordinators were also responsible for preparing position papers supporting their arguments. These position papers constitute this chapter.

After the debate on each of the three issues, a general discussion followed in which the entire team attempted to judge the relative strengths of the pro and con arguments. While these discussions mostly resulted in an impasse as far as completely endorsing or rejecting either the pro or con arguments, the weaknesses of the arguments were clearly identified.

The overall purpose of our debates was of course to resolve the issues chosen for debate. However, these issues are controversial either because of a lack of adequate experimental data or because of a lack of adequate theoretical developments. Therefore a diminished, but much more realizable goal of our debates, is to identify the loose ends in our observations, so that pertinent follow-on experiments to SMM can be devised, and to bring into sharp focus the limitations of the relevant theory and to identify what needs to be done to improve it.

The topics chosen for debate are given below in debate form:

Issue 1—Resolved: The blue-shifted components of X-ray spectral lines are signatures of "chromospheric evaporation". (Evaporated plasma is defined as cool chromospheric plasma that is heated to multimillion degree temperatures and therefore contributes to the X-ray emission of the soft X-ray flare. In the process of heating it moves upward from the chromosphere and fills coronal flux tubes.)
Sub-team coordinators for Issue 1—For: E. Antonucci, Against: G. A. Doschek

Issue 2—Resolved: The excess line broadening of UV and X-ray lines is accounted for by a "convective velocity distribution" in evaporation.
Sub-team coordinators for Issue 2—For: S. K. Antiochos, Against: D. M. Rabin

Issue 3—Resolved: Most chromospheric heating is driven by electron beams.
Sub-team coordinators for Issue 3—For: G. H. Fisher, Against: D. M. Rust

4.1.1 Rationale for Issue 1

One of the key experiments on SMM is the X-ray crystal spectrometer experiment (the XRP). The crystals in the spectrometer represent a quantum leap in spectral resolution compared to the crystals flown a decade ago by NASA on the Orbiting Solar Observatories (OSOs). Due to their high resolution and relatively high sensitivity, profiles of X-ray lines can be obtained with fairly good time resolution throughout the course of a soft X-ray (SXR) flare. Crystal spectrometers with essentially the same resolving power have

also been flown on the DoD P78-1 spacecraft and on the Japanese Hinotori spacecraft.

These crystal spectrometer experiments have resulted in important extensions of observations concerning flares. One observation is that during the rise phase of flares the profiles of X-ray lines exhibit a blue-shifted component, characteristic of velocities between 100 and 500 km s^{-1} (Doschek *et al.*, 1980, Antonucci *et al.*, 1982). The intensity of the blue-shifted component is usually much less than the intensity of the non-Doppler shifted, or stationary component, throughout the rise phase of flares. However, for a few events the intensity ratio may be about 0.5 or greater at the onset of the events.

The observation of anisotropic bulk motions of high temperature plasma ($T > 2 \times 10^6$K) is not new, and was reported in the analysis of previous X-ray (Korneev *et al.*, 1980) and XUV data (Widing 1975). However, the time relationship of this emission to the emission from the bulk of the SXR emitting plasma could not be determined from the small number of observations of large flares. In addition, a number of other interesting characteristics of the blue-shifted emission have been found by Antonucci and Dennis (1983) and Antonucci, Gabriel, and Dennis (1984) from analysis of SMM data, assuming a two-component model composed of a stationary component, and a single blue-shifted component. Although the actual distribution of velocities in the flare plasma might involve more than two components, or in fact be a continuous distribution of velocities, the two-component approximation has been illuminating regarding the intensity and magnitude of the blue-shifted emission.

The two most important questions regarding the blue-shifted component are what is its origin, and what is the relationship of the blue-shifted emission to the stationary SXR emission. Doschek *et al.* (1980) suggested that the blue-shifted emission might be the signature of the "primary chromospheric evaporation" discussed by Antiochos and Sturrock (1978), but cautioned that the blue-shifted emission might also be a phenomenon similar to a surge, not necessarily physically associated with the magnetic loops that contain the bulk of the SXR plasma. The spectrometers on the P78-1 spacecraft lacked any spatial resolution, and therefore Doschek *et al.* (1980) could not distinguish between these two possibilities. The SXR spatial resolution of the SMM spectrometers is only $\simeq 17''$, which is also not sufficient to distinguish between the two explanations.

Nevertheless, based on the presence of the blue-shifted emission during the rise phase of a large percentage of the flares observed by SMM, Antonucci *et al.* (1982) interpret the blue-shifted emission as chromospheric evaporation. That is, they propose that the primary flare energy release occurs in coronal flux tubes. Part of this energy is subsequently deposited by either conduction or transport by high energy particles into the chromosphere. This results in heating the chromosphere to multimillion degree temperatures. The heated gas moves upward into the flaring flux tubes, and the Doppler effect causes the X-ray emission from this upwelling plasma to be blueshifted relative to non-moving or stationary plasma already present in the flux tubes. The ablated or evaporated plasma is the main cause of the increase in emission measure of the SXR flare. This point of view was challenged by some members of the team. They felt that a close comparison of the characteristics of the blue-shifted emission to what is expected or predicted by numerical simulations of chromospheric evaporation revealed disturbing discrepancies. Resolving the origin of the blue-shifted emission is the primary reason for debating Issue 1.

4.1.2 Rationale for Issue 2

The reason for debating Issue 2 also revolves around the idea of chromospheric evaporation, and in addition is based on another important finding from the X-ray spectra. This concerns the considerable degree of turbulence found in flare plasma during the rise phase of SXR flares (e.g., Doschek, Kreplin, and Feldman 1979, Antonucci *et al.*, 1982). The temperature of the plasma that we are referring to here is $> 6 \times 10^6$K and $< 3 \times 10^7$K. This is the temperature range of the so-called thermal flare plasma. The fact that considerable turbulence exists in flares is in itself not new and was discovered in the analysis of the high resolution X-ray spectra analyzed by Grineva *et al.* (1973) and was also found in the analysis of XUV Skylab data (e.g., Brueckner 1976, Cheng 1977). However, the new instruments have allowed the magnitude of the turbulence as a function of time during a flare to be determined, for a large number of flares.

The origin of this turbulence is unknown, and perhaps the term "random mass motion" is more appropriate. For the sake of brevity the term turbulence is adopted, with the caveat that the origin of the broadening may not be turbulence in the strict plasma physics definition of the word. It does not appear that the excess line widths are due to ion temperatures that are much higher than the electron temperature. The electron temperature is well-determined and therefore it is possible to compute the implied difference in ion and electron temperature accurately. At the known electron density of SXR flare plasmas, it is difficult to explain how this difference in temperature could be maintained over the observed intervals of flare rise times. Also, the quantity $\Delta\lambda/\lambda$, where $\Delta\lambda$ is the line width and λ is the wavelength, scales as $1/\sqrt{M_I}$ where M_I is the ion mass, if the broadening is predominately due to Doppler ion broadening. However, the observed values of $\Delta\lambda/\lambda$ are independent of ion mass, thus supporting the random mass motion interpretation. Therefore most investigators have assumed that the broadening is due to mass motions, and not instead due to an ion temperature that is much higher than the electron temperature.

It is a difficult task to answer the general question, what causes the non-thermal broadening of X-ray lines, since there are many possibilities, such as true plasma turbulence or sim-

ply spatially non-uniform heating in flux tubes which would produce hydrodynamic turbulence. Another possibility that the team thought interesting to investigate is that the turbulence is due to the distribution of velocities produced in chromospheric evaporation. More specifically, in the evaporation process plasma at a given temperature evaporates with a range of speeds. This is one of the results of numerical simulations, and would produce Doppler broadening of spectral lines. This occurs even in one dimensional (1D) numerical simulations. The reason for investigating this particular possibility is that it is possible to use numerical simulations to calculate the expected broadening. A similar calculation is very difficult for some of the other likely mechanisms, such as plasma turbulence. There are simply too many undetermined parameters to make meaningful calculations of all plausible broadening mechanisms. The team felt that it might be possible to determine whether or not convective evaporation is a viable broadening mechanism and therefore decided to debate the issue. Issue 1 and Issue 2 are intimately related.

4.1.3 Rationale for Issue 3

For some time now the relative importance of electron beams and conduction fronts in heating the flare chromosphere has been debated by the general solar physics community. A number of numerical simulations of chromospheric evaporation have been carried out (e.g., Nagai 1980, Cheng *et al.*, 1983, MacNeice *et al.*, 1984, Pallavicini *et al.*, 1983, Fisher, Canfield and McClymont 1985b,c). These simulations contain *ad hoc* heating functions either in the form of coronal heating transported by conduction fronts or electron beams that deposit their energy in the chromosphere. At first sight it is not clear from these papers whether conductive heating or beam heating provides the closest correspondence to observational data. However, detailed comparisons of temperatures and upflow velocities from these model calculations do show significant differences between the two types of flare heating (Fisher, Canfield, and McClymont 1984). Furthermore, detailed modelling of the chromosphere and transition region has produced observational tests which can be used to study the spatial distribution of heating in flares (Canfield, Gunkler, and Ricchiazzi 1984, Fisher, Canfield, and McClymont 1985b,c).

The presence of an electron beam is inferred from the hard X-ray (HXR) bursts that frequently occur during the impulsive phase of flares (during the rise phase of SXRs). The SMM, P78-1, and Hinotori spacecraft carry HXR broadband spectrometers in addition to the crystal spectrometer experiments. A question of considerable importance to flare theory is whether the energy contained in a possible electron beam is sufficient to power the SXR event. Is the energy released in the chromosphere by the beam sufficient to drive chromospheric evaporation and produce the initial emission measure growth of the SXR flare? Feldman, Cheng, and Doschek (1982) argue that the HXR emission represents an energy release mode that is coincidental in time to, but not the cause of, the production of the SXR flare. They argue that the HXRs and SXRs are produced by a common energy release mechanism, but are otherwise unrelated, i.e., the energy in the nonthermal electrons does not power the SXR flare. Other investigators, while disagreeing with the position of Feldman, Cheng, and Doschek (1982), nevertheless also feel that the energy contained in electron beams is insufficient to power the SXR flare. They feel that chromospheric evaporation produces the SXR event and is caused by heating originating in coronal loops which propagates via conduction downward into the chromosphere. Because of the fundamental importance of these questions to the understanding of energy transport in flares, the team decided to debate Issue 3.

Finally, before commencing with the debate issues in Sections 4.3, 4.4, and 4.5, a brief description of the X-ray crystal spectrometer experiments is given in Section 4.2, since the data from these experiments are central to both Issues 1 and 2.

4.2 CRYSTAL SPECTROMETER EXPERIMENTS

The first high resolution solar spectra from hot plasmas were obtained by Grineva *et al.* (1973), from a few flares during 1970. The iron lines between 1.85 - 1.87 Å were observed with two quartz spectrometers on the Intercosmos-4 satellite, launched on October 14, 1970. The spectra were obtained with a resolution of 0.4m Å by scanning the solar disk with the satellite axis. The most important lines in the 1.85 - 1.87 Å range were identified using these spectra (Grineva *et al.*, 1973, Gabriel 1972). However, emission from Fe II - Fe XXIII was not observed with high resolution.

The SOLFLEX (Solar Flare X-rays) experiment consists of four Bragg spectrometers operating in the interval 1.8 - 8.5 Å, where important SXR spectral lines are found. It was flown by the Naval Research Laboratory (NRL) on an Air Force spacecraft called P78-1, which was launched on February 24, 1979. A wavelength scan is completed by this instrument in about 56 seconds. The effective time resolution is variable and can be as short as about 10 s. Another crystal spectrometer experiment flown on P78-1 is the SOLEX (Solar X-rays) spectrometer package, built by the Aerospace Corporation. These crystals scan the longer wavelengths between 5 and 23 Å. The P78-1 instruments have been described recently by Doschek (1983).

The Soft X-ray Polychromator experiment (XRP) consists of two instruments: the Bent Crystal Spectrometer (BCS) and the Flat Crystal Spectrometer (FCS) (Acton *et al.*, 1980). It was built by groups at Lockheed, Culham Laboratory, and the Mullard Space Sciences Laboratory and was flown on the Solar Maximum Mission satellite, which was launched on February 14, 1980. The Bent Crystal Spectrometer con-

sists of eight curved crystals and position sensitive detectors to achieve high time resolution (effective time resolution of 1 second) as well as high spectral resolution. The spectrometer detects the SXR emission in the interval 1.77 - 3.23 Å. The Flat Crystal Spectrometer has seven Bragg crystals which simultaneously diffract X-rays in seven different wavelength regions in the interval 1.4 - 22.4 Å.

Two rotating crystal spectrometers, called SOX1 and SOX2, were flown by Tokyo University on the Hinotori (Astro-A) satellite launched February 21, 1981. These spectrometers observe the two wavelength ranges 1.72 - 1.95 and 1.83 - 1.89 Å (Tanaka *et al.*, 1982a). They are flat spectrometers and the wavelength range is scanned by using the spin of the spacecraft itself. The time resolution is comparable to the effective time resolution of the BCS.

The spectrometers on the P78-1, SMM, and Hinotori satellites have operated continuously for many months, giving a large set of observations of intensities and profiles of lines, emitted by plasma at temperatures greater than 10^7 K, formed during solar flares. The spectral resolution of all these spectrometers is sufficient for measuring spectral line profiles. The intensities of lines are important for determining the electron temperature, electron density, emission measure distribution, and departure from ionization equilibrium. The spectral regions most studied are the wavelength bands near the resonance lines of helium-like iron (Fe XXV, 1.85 Å) and calcium (Ca XIX, 3.176 Å).

4.3 DEBATE OF ISSUE 1

The debate of Issue 1 began by defining precisely what is meant by chromospheric evaporation. The term was defined to mean the heating of chromospheric plasma to soft X-ray emitting temperatures by either thermal conduction and/or electron beams, and its consequent expansion upward into flux tubes. The evaporating plasma is rapidly heated to temperatures $> 10^7$ K, thereby producing the large SXR emission measure. The sub-team presenting the argument for the interpretation of the blue-shifts as indicators for chromospheric evaporation asserts that the evaporated plasma is the major cause of the increase of SXR flux and emission measure. The sub-team presenting the case against this interpretation did not attempt to claim that no upward moving plasma exists, but their contention is instead that the blue-shifts are not the major cause of the large SXR emission measure increase.

4.3.1 Argument for: The Blue-shifts Are Direct Evidence of Chromospheric Evaporation

The sub-team arguing for a chromospheric evaporation interpretation of the blue-shifts list several properties of the blue-shifts that either support or are consistent with this interpretation. Previously, the profile of the Fe XXV resonance line was reported to be broadened, indicating turbulent motions of the order of 90 km s^{-1}, from observations obtained from the Intercosmos-4 satellite (Grineva *et al.*, 1973). Most of the spectra were recorded during the peak or the decay phase of flares except for two obtained during the rise time. For the rise phase spectra a shift of the Fe XXV resonance line toward the blue was also observed, which implied motion of the SXR source toward the observer with velocities of 160 km s^{-1}. If line shifts are observed in peak phase or decay phase spectra, they are toward the red and the downward velocities deduced are of the order of 200 km s^{-1} (Korneev *et al.*, 1980). An absolute wavelength calibration is available for these data.

From the line width analysis of several flares of class M and X observed with the SOLFLEX spectrometers, Doschek *et al.* (1980) and Feldman *et al.* (1980), conclude that line profiles are broader than the thermal width, computed from the electron temperature determined from the dielectronic satellite lines. The widths are greatest at flare onset, and decrease monotonically during the rise phase. Near maximum X-ray flux the broadening has decreased considerably. This effect is more evident in class X flares. In the decay phase of M and X flares the lines are narrower, with nonthermal velocities of about 60 km s^{-1}. The line broadening at flare onset is characterized by a nonthermal velocity parameter of about 150 km s^{-1}. Doschek *et al.* (1980) also reported the existence of a weak blue-shifted emission component of the Ca XIX resonance line, that was only apparent during the rise phase of X-class flares.

Two of the M flares reported by Feldman *et al.* (1980) show a relatively strong component of plasma (compared to non-moving plasma) moving outward from the sun at velocities of about 400 km s^{-1}, with a temperature probably near 15×10^6 K. This result is based on the observation of a blue-shifted component of both the Ca XIX and Fe XXV resonance lines, which has the form of an asymmetrical extension on the blue-wings of the lines. The blue-component is strongest in the earliest rise phase spectra. The X-ray flux in these spectra is about 50% of the flux in the stationary component. The flux of the dynamic component tends to slightly increase or remain constant during the flare rise phase. After flare maximum it is either very weak or absent. The dynamic and static components of the resonance line of Ca XIX are deconvolved under the assumption that both components produce Gaussian profiles. Wavelength shifts of the resonance line itself, as observed by Korneev *et al.* (1980), are not discussed by these authors.

The high time resolution observations of the flare SXR emission, obtained with the Bent Crystal Spectrometer on SMM, confirm that the X-ray line profiles of ions such as Ca XIX are broad and complex. These properties of the lines are found to be a systematic characteristic of the impulsive phase of flares (Antonucci *et al.*, 1982). A more detailed discussion of the properties derived from BCS data is given

in Subsection 1. The results obtained from the Hinotori observations in general confirm the existence of non-thermal profiles and blue extensions of spectral lines. Non-thermal velocities of about 200 km s^{-1} and upward velocities of about 400 km s^{-1} are derived at flare onset (Tanaka *et al.*, 1982a,b).

4.3.1.1 General Properties of the Plasma Upflows

The general properties discussed above have been studied systematically using a large set of spectra observed during the rise phase of class M and X flares obtained with the BCS on SMM during 1980 and the results appear to be consistent with the hypothesis of chromospheric evaporation (Antonucci 1982, Antonucci and Dennis 1983, Antonucci, Gabriel, and Dennis 1984).

Evaporation occurs in response to local chromospheric heating as a consequence of the primary energy release during a flare, and as predicted by different models, it can be produced either by electron beam heating or conductive heating of the chromosphere. In the case of beam heating, the energy release is associated with emission in hard X-rays. Under the hypothesis that the blue-shifted components are due to chromospheric material heated during the energy release and driven up along the magnetic field lines, and considering the HXR impulsive emission as a temporal indicator of this energy deposition, upflows are expected as long as the impulsive HXR emission is observed. While evaporation takes place, the magnetically confined plasma accumulates in coronal flux tubes. The velocity of the evaporating plasma has to decrease with the increase in density of the plasma accumulating in the coronal region, because of the decrease in pressure difference between the chromosphere and the overlying coronal flare loop. In general, correlations between the parameters of the static and the dynamic components of spectral lines are expected, because in the theory of chromospheric evaporation they are causally related. Chromospheric evaporation is also expected to be related to the sites of energy deposition, that is at the footpoints of the flaring coronal loops.

The observational properties of the X-ray lines of class M and X flares confirm the above picture. In about 80% of the disk flares detected with the BCS, a blue-shifted component was observed in association with the spectra emitted during the impulsive phase. This component is absent in the emission of flares occurring beyond about 60 degrees in longitude. This indicates the presence of flows of a part of the SXR emitting plasma that are mainly upward. The observed upward velocities can be as high as 300-400 km s^{-1} at flare onset and they decrease during the rise of the soft X-ray flux. In the decay phase, the dynamic blue-shifted component of the SXR source is no longer observed. (Shifts between spectral components corresponding to velocities below 120 km s^{-1} cannot be measured reliably).

In both disk and limb flares, large non-thermal line broadenings are observed during the rise phase, and in general are insignificant during the decay phase. Upflows and non-thermal motions observed during the rise of the SXR emission are also observed simultaneously with the most intense HXR emission above 25 keV. This indicates a causal relation among the different phenomena, in particular, the HXRs, the SXRs and the plasma upflows, as expected if chromospheric evaporation is present. SXR and HXR emissions, from the region of the May 21, 1980 flare, are shown in Figure 4.1 as an example. Defining the parameter Δ T as the difference between the Doppler and electron temperature, and defining v′ as the velocity of the dynamic component of the SXR source, it can be seen that these quantities deviate considerably from zero during the impulsive SXR emission and the rise of the SXR flare. Both quantities moreover are largest at flare onset and decrease during the impulsive phase. They are negligible at flare maximum. Line-broadening motions in general precede line-shifting motions in a flare, as shown in the example of Figure 4.1. The quantity Δ T is taken here and subsequently as an indicator of nonthermal *broadening,* as opposed to line-shifting.

While the upflow velocity is decreasing, the density in the coronal region of the flare is increasing, as can be deduced from the evolution of the emission measure EM of the stationary SXR source for the event of May 21, 1980, derived assuming isothermal conditions at the electron temperature T_e. The quantities T_e and log (EM) are also shown in Figure 4.1. The temperature T_e is obtained from the intensity of the Ca XVIII dielectronic satellite lines. Since the area of the flare as observed in SXRs, in the energy band 3.5 – 8 keV of the Hard X-ray Imaging Spectrometer (HXIS), does not change significantly during most of the impulsive phase, the increase in EM indicates a simultaneous increase in electron density of the flare plasma.

The emission of the material associated with the high speed upflows is in general weaker than that of the main SXR source, which produces unshifted spectral lines. Only in a few cases for a short period, on the order of 20 seconds at flare onset, is the intensity of the blue-shifted emission observed to be equal to that of the primary (unshifted) emission. Both of these emissions increase in absolute flux, although the flux of the dynamic component decreases with respect to the primary one during the impulsive phase (Antonucci, Gabriel, and Dennis 1984).

The upward velocities observed during the impulsive phase for the dynamic plasma component are correlated with the average rate of increase of the emission measure of the coronal plasma, with a correlation coefficient of 0.8. In addition the peak emission measure of the upward moving plasma is also positively correlated with the peak emission of the principal coronal source emitting SXRs, with a correlation coefficient of 0.7 (Antonucci and Dennis 1983). The flare properties presented up to now are quite general.

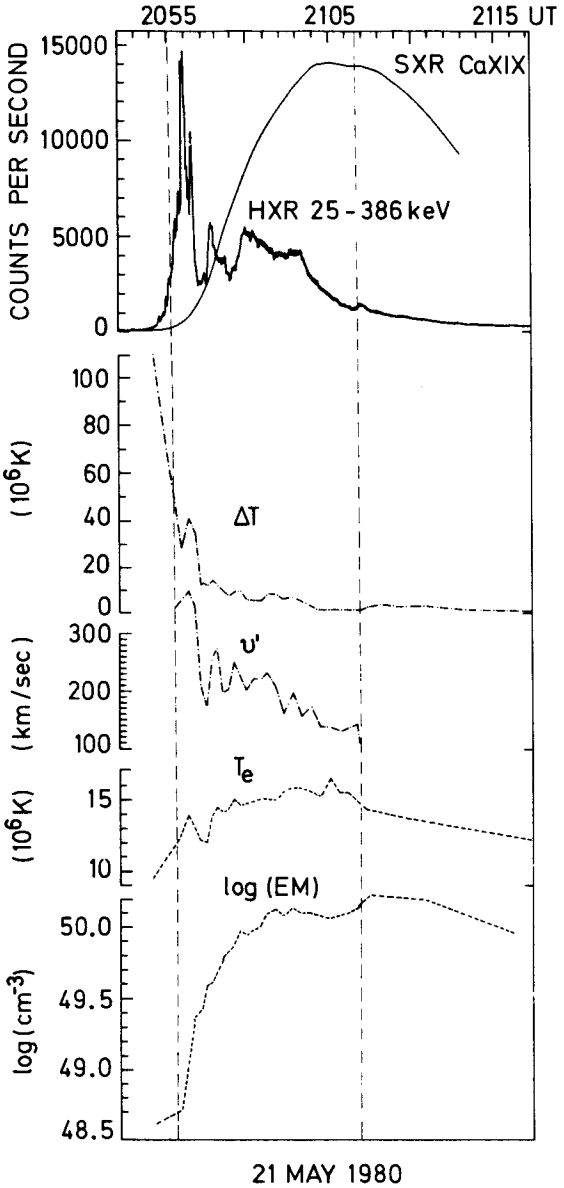

Figure 4.1 Temporal evolution of the following observed quantities for the flare on May 21, 1980: the SXR calcium line emission detected with the Bent Crystal Spectrometer integrated over the spectral range 3.165 to 3.231 Å; the HXR emission detected with the HXR Burst Spectrometer in the energy range from 25 to 386 keV; the parameter ΔT indicating the amount of nonthermal broadening in the line profiles, expressed in terms of equivalent temperature excess; the velocity v′ of the high speed upflows; the electron temperature T_e; and the logarithm of the emission measure EM of the principal SXR source. The last four physical parameters were derived from the analysis of BCS spectra in the Ca XIX channel, similar to the one shown in Figure 4.2. Upflows with $v' \gtrsim 120$ km s^{-1} are observed during the time interval indicated by the dashed vertical lines.

In a few events it is also possible to observe, in addition to the blue-wing asymmetry or the blue-shifted component, a blue-shift of the resonance line of the primary component itself, as reported by Korneev *et al.* (1980). In the case of the May 21 event, the blue-shift of the dominant component is observed before the blue-shifted component appears (see discussion in Subsection 2).

4.3.1.2 SXR Line Spectra During the Impulsive Phase

The results presented in Subsection 1 are well illustrated by a sequence of calcium spectra detected during the May 21 flare, in Figure 4.2. The first significant SXR emission detected in the BCS spectral band from 3.165 to 3.231 Å, where the Ca XIX resonance line and its associated satellites are observed, in Figure 4.2a, is an average over 120 seconds. The emission is integrated over the entire flare region, since the BCS field of view is 6 arc min × 6 arc min. The emission measure of the source at this time is approximately 5×10^{48} cm^{-3}. Although the counting rate is low, approximate values can still be derived for the Doppler and electron temperatures as described later. The resonance line is significantly broadened with a Doppler temperature of about 1.3×10^8 K. This broadening must be nonthermal in origin since it would imply an ion temperature of one order of magnitude larger than the electron temperature, which is about 9×10^6 K. Hence nonthermal motions with a mean velocity of 220 km s^{-1} are expected in the flaring region.

The subsequent spectrum, in Figure 4.2b, shows the appearance of a blue-shifted component; the only observable unblended feature is on the blue side of the resonance line, i.e., the line at 3.177 Å. (This line is at the location of the vertical dashed lines in Figure 4.2.) The intensity of this feature exceeds by 7 standard deviations the intensity expected from the profile of the unshifted resonance line, i.e., the dashed profile in Figure 4.2b, computed for a Doppler temperature of 4×10^7 K. The two lines have comparable intensities and the relative blue-shift of the new feature is 3.8 mÅ, a value which implies high speed plasma flows with a line-of-sight velocity of about 360 km s^{-1} relative to the principal source. The line-of-sight is approximately radially outward since the flare occurred near disk center at S14, W15. In the spectrum of Figure 4.2c, the blue-shifted emission has decreased in intensity relative to the unshifted component with unchanged line-of-sight velocity. The line spectrum continues to consist of two components until the SXR emission reached its peak intensity at 21:07 UT. After this time it disappears, and the excess widths of the line profiles (over the thermal Doppler widths), assumed to be produced by nonthermal motions, disappear as well. Figure 4.2d shows an example of the one-component spectrum with thermal line profiles.

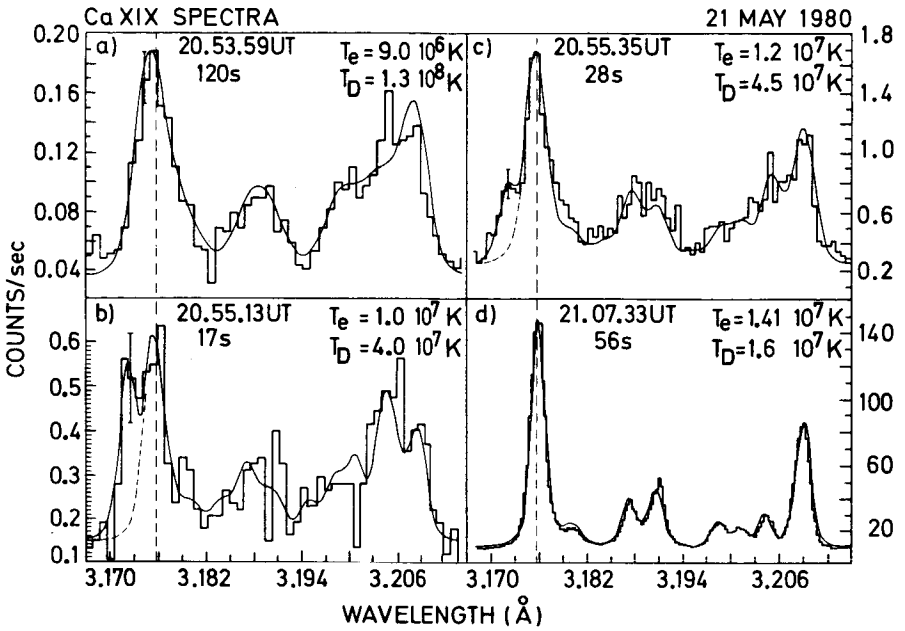

Figure 4.2 Sequence of SXR spectra obtained at four different times during the impulsive phase of the May 21, 1980 solar flare by the BCS in the Ca XIX spectral region. The last spectrum was recorded at the end of the impulsive phase. The smooth curve in each figure represents the synthesized spectrum computed for given values of the electron temperature T_e and the Doppler temperature T_D. The spectra shown in b and c are the sum of two synthetic spectra, one blue-shifted by 3.8 mÅ. The dashed lines represent the profile of the principal component expected for a given Doppler temperature. The time intervals represent the effective data accumulation periods. The times of the spectra are the mean times of the observation interval.

The principal component of the resonance line is itself blue-shifted during the early stages of the flare. The BCS has no absolute wavelength calibration and this effect is deduced by studying the relative wavelength shifts of the Ca XIX resonance line during a flare. The blue-shift can be determined by comparing the wavelength at the peak of the resonance line in Figure 4.2d, indicated with a vertical dashed line, with the corresponding peak wavelength in Figures 4.2a, b, c, and it is of the order of 0.8 mÅ. The corresponding speed of the plasma flow, about 80 km s^{-1}, decreases with time from this value and the effect is observed only in the early part of the impulsive phase. The high speed upflows, giving origin to the blue-shifted component, are observed later, in coincidence with a significant increase in the rise of the HXR emission. The initially observed 80 km s^{-1} upflow is interpreted as upward motion of the entire SXR source.

The theoretical spectra that best fit the data, shown as a continuous line superposed on the observed counting rates, are obtained from a synthesis of lines, computed for given electron and Doppler temperatures, following the technique described by Antonucci *et al.* (1982). Due to the large non-thermal broadenings and the low counting rates, the spectra detected early in a flare do not present well-resolved features. However, an estimate of the order of magnitude of the physical parameters is still possible. The two-component spectra, observed when the secondary spectrum is emitted by the high velocity plasma component, are fitted by the sum of two spectra, assuming the same source parameters for the two different sources. In general the impulsive phase spectra observed with the BCS are adequately fitted by a two component synthetic spectrum as in Figure 4.2c.

4.3.1.3 Spatial Location of the Upflows and the Site of Chromospheric Evaporation

In some flares, the simultaneous detection of the SXR spectral lines with the BCS and the SXR HXIS images in the 3.5 – 8 keV energy band enable the location of the SXR source to be determined at the time when the first upflows are observed. The HXIS, described in detail by van Beek *et al.* (1980), has 8″ spatial resolution. In a few cases this instrument has resolved separate sources of 16 – 30 keV

X-ray emission early in the impulsive phase. These sources have been identified with the footpoints of magnetic loops (Hoyng *et al.* (1981), Duijveman, Hoyng, and Machado 1982). The images observed during the May 21 event shown in Figure 4.3, indicate that at the time of the appearance of the high speed mass flows at 20.55.13 UT (second spectrum of Figure 4.2) the SXR emission is concentrated mainly at sites bright in SXRs, which presumably correspond to the footpoints of coronal loops. In Figure 4.3, the images of the SXR sources are compared with those of the HXR sources in the energy band 16 – 30 keV. These images were obtained during the development of the flare impulsive phase. The HXR bright points A and B are known to coincide with regions of opposite magnetic polarities and have been interpreted as the locations of incidence of beams of accelerated particles in the chromosphere early in the flare. Hence if this interpretation is correct, the SXR plasma and the high speed plasma upflows are spatially coincident with the sites of local chromospheric heating, when they are first observed. The HXR sources A and B presumably consist of a complex of unresolved sources, corresponding to a loop system connecting areas of different polarity. The coronal regions of the loops are still at low density, since the emission is weak between the footpoints.

At earlier times during the same event, in an interval of 120 seconds around 20.54.02 UT when the first spectrum is observed, the SXR emission is already predominately concentrated at footpoint A, which remains the brightest until footpoints are observed. The presence at this time of a single spectral component, blue-shifted with respect to the rest wavelength, suggests that most of the emitting plasma is evaporating from A at low velocity in response to an initial heat input, simultaneous with HXR emission of moderate intensity.

The outward motion of the SXR source is observed for about three minutes. In approximately the same period, the centroid of the SXR emission moves from A to an intermediate position between the footpoints, in Figure 4.3. This change in configuration is consistent with the travel time to the coronal region of both the low and high speed upflows, which appear later on. The emission peak is interpreted as observed between A and B because of the density increase in the coronal region of the loop, since the evaporated material has reached the loop apex and accumulation has begun (Antonucci *et al.*, 1984, Antonucci, Marocchi, and Simnett 1984).

The plasma injected at low velocity at flare onset is negligible in the total energy budget of the SXR flare, which is predominantly formed by the plasma moving at higher velocity. However, this phase is important for clarifying the initial conditions of the loops where chromospheric evaporation occurs. These loops are initially at low density except at the base. The precise initial density of the loops is unknown.

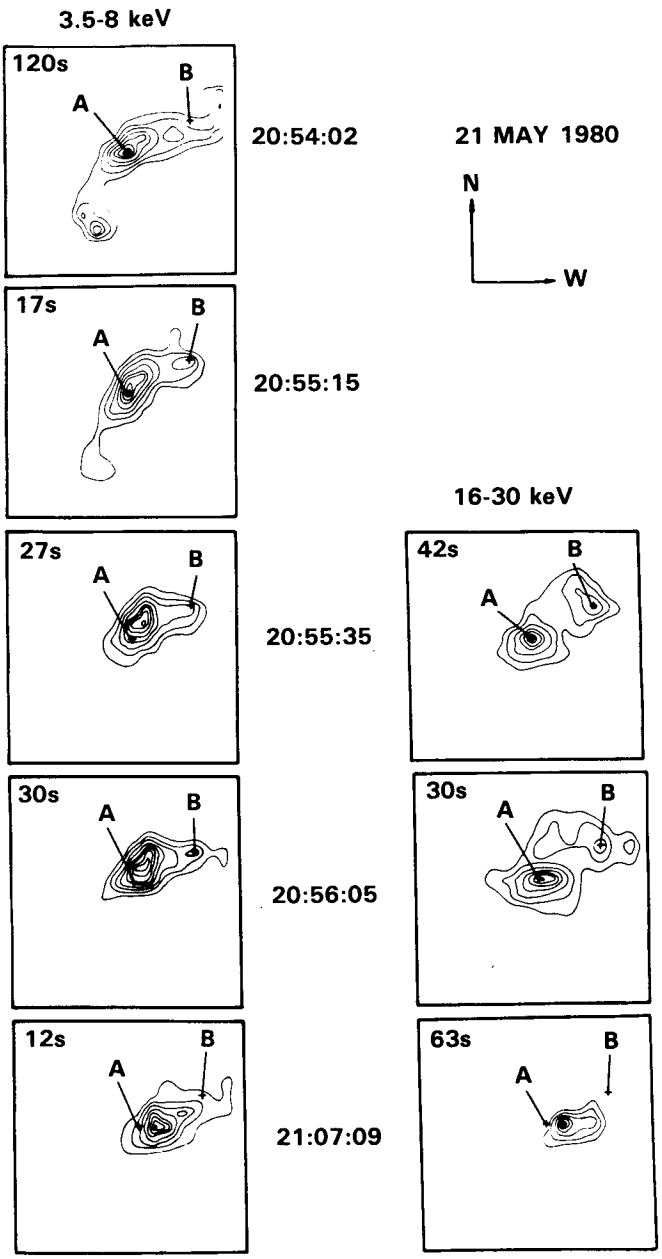

Figure 4.3 X-ray images of the flaring region, for the May 21, 1980 event, in the softer (3.5-8 keV) and harder (16-30 keV) energy bands of the HXIS. The contour levels correspond to 14, 26, 40, 55, 70, 80, 90, 98, 100% of the peak counting rate. For the hard X-ray images, the lowest contour level is 26%. The time intervals for data accumulation and the mean times of the images are shown. All images are deconvolved to allow for the triangular response of the HXIS collimator. The crosses represent the peak of the HXR emission at the two footpoints A and B, as measured in the first X-ray image in the energy band from 16 to 30 keV. This image is averaged over a period covering the two SXR images at 20.55.15 and 20.55.35 UT.

In addition, this phase corresponds to a low or moderately low value of the derivative of the observed HXR emission. Correspondingly, the energy flux, heating the chromosphere, increases slowly at first. This is probably the reason for an evaporation evidenced by a single component, indeed blue-shifted but by a small amount, which can be difficult to measure because of line-of-sight effects. In numerical simulations of flaring loops, the temporal profile of the energy input to the chromosphere should be chosen to simulate that inferred from the HXR emission, since it may be quite important in reproducing more accurately the observed flare profiles.

Under the interpretation given above, the dominant plasma source becomes stationary at the loop apex. However, it is still possible to infer from where evaporation occurs. This is done by comparing the ratio of the flux of the shifted to the unshifted spectral component, observed by the BCS, to the ratio of the SXR emission between 3.5 – 8 keV that arises from the two areas bright in HXRs, and identified with the footpoints, to the diffuse emission that arises between the footpoints, observed by HXIS. This test has been applied to the April 10, 1980 flare, a well-observed event discussed by Antonucci *et al.* (1982). The results suggest that during the impulsive phase the principal component in the BCS spectra is due to the emission integrated over the volume of the magnetic loop connecting the footpoints, while the blue-shifted component is localized in the proximity of the footpoints.

Referring now to earlier Skylab data, Hiei and Widing (1979) studied an event that occurred on January 21, 1974 that was optically classified as a—N subflare. This flare appears as a brightening of a single well-resolved loop. The position of the maximum electron density derived from the intensities of the Fe XV diagnostic lines, i.e., the maximum density at the temperature of formation of Fe XV, moves from one foot of the magnetic arch to the top of the loop with time. The concentration of the plasma near the footpoint at the beginning and its subsequent motion suggest that material is supplied from the lower atmosphere. The plasma in this case does not reach temperatures of 1×10^7 K. The transition region lines show blue-shifts corresponding to line-of-sight velocities of 120 km s^{-1}.

4.3.1.4 Energetics of Chromospheric Evaporation

For a definitive identification of upflows with evaporated chromospheric material, and to conclusively demonstrate that evaporation is the principal process in the formation of the SXR source in the coronal region, a detailed quantitative analysis is needed. With the data available, the amount of hot material supplied to the corona by the upflowing plasma cannot be established directly, since the amount of mass, enthalpy, and kinetic energy flowing into the coronal region cannot be derived from the parameters obtained from the SXR spectra alone.

However, the hypothesis of chromospheric evaporation can be indirectly explored by determining under what conditions the increase in emission in the principal spectral source, assumed to represent the coronal plasma, is consistent with the observed plasma upflows (Antonucci, Gabriel, and Dennis 1984). This is done under the assumption that the upflows are completely magnetically confined. It is also assumed that the plasma is flowing into the confinement region through the footpoint areas.

Only the average velocity v' and the average emission measure EM', of the upflowing plasma can be deduced with sufficient accuracy for the evaporating material. The temperature T_e' and the density n_e' of the upflow, however, can be derived indirectly. This is done by requiring that the material evaporating through the footpoints of the flaring loops supply sufficient mass and energy to account for the mass and thermal energy in the static coronal source at the end of the evaporation process. The physical conditions of the coronal source are well-defined except for those quantities that depend on the source volume. Upper limits to the volume can be inferred from the flare images obtained with the HXIS. Coronal loop footpoints, the most probable sites of chromospheric evaporation, can be identified from the impulsive phase HXR emission in the HXIS images, for a few flares reported in Tables 4.1 and 4.2. For these flares the upper limits to the footpoint cross-sections and distances between the footpoints are approximately known, and are selected for this quantitative test.

Following an approach described in Antonucci *et al.* (1982), the density of the upflowing plasma is derived by requiring that the integral of the electrons flowing in unit time through the two footpoints is equal to the increase of the electron number in the confining region during the evaporation time. Once n_e' is known, T_e' can be derived by requiring that the integrals over time of the enthalpy and kinetic energy transported by the upflowing plasma into the coronal region in unit time are equal to the simultaneous increase in the total thermal energy of the SXR emitting source. The total energy input corresponds to the sum of the thermal and turbulent energy increases during the evaporation process and of the energy losses, summed from flare onset. The energy losses of the coronal part of the loop are conduction to the chromosphere and *in situ* radiation from the coronal region.

The values of the electron density of the coronal plasma at the onset and at the end of the evaporation process, n_{e1} and n_{e2} respectively, and the peak values of the electron temperature T_e, are compared in Table 4.1 with the derived T_e' and n_e' values for the evaporating plasmas. The quantities T_e' and n_e' are average values over the evaporation period. For each quantity a range of values is given to account for the uncertainty of the inferred volume and to quantify the degree of dependence of the results on the flare volume. They correspond to a range of volumes within two limiting

Table 4.1 Densities and Temperatures of the Coronal and Upflowing Plasmas

Flare 1980	T_{max} UT	n_{e1} 10^{11} cm^{-3}	n_{e2} 10^{11} cm^{-3}	n_e' 10^{11} cm^{-3}	T_e' 10^7 K	$T_{e,peak}$ 10^7 K
8 April	03.07	0.9-0.5	3.1-1.6	0.5-1.0	1.6-1.1	1.5
10 April	09.22	1.0-0.7	3.3-2.1	1.1-1.8	1.2-0.9	1.6
9 May	07.14	1.5-1.1	6.4-4.8	1.5-2.0	1.5-1.2	1.8
21 May	21.07	0.5-0.2	2.6-0.8	0.4-1.4	1.8-1.0	1.7
5 Nov	22.36	0.9-0.3	2.0-0.7	0.5-1.3	3.0-1.8	2.0

T_{max} — time of maximum emission.

n_{e1}, n_{e2} — electron densities of the coronal plasma at the onset and at the end, respectively, of the period of observed blue-shifts.

n_e', T_e' — electron density and temperature, respectively, of the upflowing plasma averaged over the period of observed blue-shifts.

$T_{e,peak}$ — peak value of the electron temperature of the coronal plasma.

The two values given for the densities and for T_e' correspond to the upper and lower limits on the volume (see explanation of Table 4.2).

Table 4.2 Energetics of Flares with Hard X-ray Footpoints

Flare Date	Soft X-Ray Coronal Plasma		Hard X-Rays
1980	ΔE_{SXR} 10^{30} ergs	ΔE_{tot} 10^{30} ergs	ΔE_{HXR} 10^{30} ergs
8 April	2.9-3.9	5.3-4.5	9
10 April	1.9-2.4	3.6-3.1	5
9 May	1.6-1.7	4.5-3.3	5
21 May	8.2-16.	13.-14.	10
5 Nov	2.7-4.7	3.1-3.4	7

Explanation of column headings

ΔE_{SXR} — increase in the total energy of the coronal plasma including the radiative and conductive losses during the evaporation process.

ΔE_{tot} — total energy in radiative and conductive losses during the flare.

ΔE_{HXR} — total energy in fast electrons with energies above 25 keV derived from the HXR observations during the evaporation process assuming thick-target interactions.

The two values given for the parameters of the SXR coronal plasma are for two different geometries. The first value was calculated assuming a lower limit V_1 to the volume taken to be that of a semicircular loop with length $\pi\ell/2$ and cross-sectional area $A = d^2$. The second value was calculated using an upper limit V_2 to the volume taken to be ℓ^3.

cases regarding the geometry of the source. In one case the source is chosen to be a semicircular loop connecting the two footpoints, and in the other case a cubic volume is assumed, where the linear dimension is taken to be the average linear extent of the SXR region.

Clearly, simple hydrodynamical considerations of the chromospheric evaporation model require that the pressure in the expanding evaporated plasma must exceed the pressure at the top of the loop. Since the temperature of the upflowing and stationary plasma are inferred to be approximately the same, this condition implies that n_e' must exceed n_e. The values tabulated in Table 4.1 for n_e' are believed to be consistent with this requirement, at least for volumes larger than a semi-circular loop. However, in this case also the results are presumably still valid. In fact, the values of n_e' are to be considered lower limits since the footpoint cross-sections are upper limits, due to the spatial resolution of the HXIS. In addition, it has been assumed that the magnetic fields completely confine the plasma flows in the corona, which is a restrictive condition. Higher densities would also result from overestimating the duration of the injection process. As shown in Table 4.1, for larger volumes, still compatible with the observed dimensions of the flare region, even the lower limit of the evaporating plasma density n_e' becomes of the same order as the peak density in the coronal plasma n_{e2}, insuring that the density n_e' is larger than the coronal density while evaporation is observed.

The continuity equations used to derive the quantities in Table 4.1 are expressed in terms of two unknown parameters: $\alpha = v'/v$ and $\beta = T_e'/T_e$, where v and T_e are respectively the volume and electron temperature for the plasma in the coronal region and v' and T_e' are the volume containing the blue-shifted component and its temperature (Antonucci *et al.*, 1982). Since the emission measure of the coronal source is higher than that of the evaporating material, the pressure requirement on the chromospheric material in order that it is able to expand into the loop implies that the parameter α is less than unity. This corresponds to a situation where evaporated plasma is confined in the lower portions of the flaring loops.

Similarly, Tanaka, Ohki, and Zirin (1985) discuss a white light flare observed on June 6, 1982, which is the largest event detected by high resolution spectrometers during the recent solar maximum. Spectral information as well as SXR images in the energy band 5 - 10 keV have been obtained by the Hinotori satellite. The flare is preceded by a filament eruption. However, the authors conclude that the upflows observed at velocities of 400 km s^{-1} during the impulsive phase are not related to this phenomenon. Non-thermal motions are present throughout the impulsive phase. Bright points, assumed to be the footpoints of the magnetic arcade where the flare occurs, are observed in Hα and D3 emissions and it is assumed that semicircular loops connect the footpoints. By requiring mass balance during the impulsive phase, the density of the evaporating material should be twice as large as that of the coronal plasma to account for its formation. That is, the evaporation hypothesis is consistent with this result, if the rising plasma is confined to a small portion of the loop arcade, presumably near the footpoints, as expected. The energy balance presents some difficulty because of the large conduction losses. These losses integrated over the flare duration exceed 10^{32} ergs (one order of magnitude larger than the maximum thermal energy), since the flare plasma is estimated to be at the relatively high temperature of 4×10^7 K. This temperature is inferred from the Fe XXVI diagnostic lines. However, conduction losses may be reduced, e.g., by magnetic constriction, to a value lower than the thermal energy.

Hence, the observations of upflowing plasmas during the rise phase of SXR emission support the hypothesis that evaporation of heated chromospheric plasma is the main source of the SXR emitting plasma confined to coronal loops. This interpretation is quantitatively confirmed if the plasma upflows have densities equal to or greater than 10^{11} cm^{-3} and temperatures of the order of $1 - 2 \times 10^7$ K.

4.3.1.5 Direct Measurement of Material Evaporated During the Impulsive Phase

Evidence for the appearance of soft X-ray emitting plasma associated with a simultaneous disappearance of chromospheric material is reported by Acton *et al.* (1982). They have determined the amount of material that has been evaporated from the chromosphere during a compact flare, classified as C7, observed on May 7, 1980. The material evaporated appears to be more than enough to account for the emission measure of all the mass content at temperatures greater than 10^6 K, measured with the SMM instruments. These results are derived from a study of the profiles of the Hα line, obtained at the Sacramento Peak Observatory vacuum tower telescope. The amount of evaporated chromospheric material is estimated through a comparison of the observed profiles with the profiles predicted by a semi-empirical model of a flare chromosphere.

The same is found for another flare observed during SMM on June 24, 1980, as reported by Gunkler *et al.* (1984). In this flare, the maximum line-of-sight velocity is 300 km s^{-1} for the evaporated plasma emitting blue-shifted SXR, observed by the BCS. The amounts of chromospheric evaporation by conduction and non-thermal electrons are calculated and both mechanisms are found to be able to account for the observed increase in the coronal density. In this work the Hα profiles are analyzed by comparison with the theoretical profiles calculated by Canfield, Gunkler and Ricchiazzi (1984).

4.3.1.6 Early Phase of Chromospheric Evaporation

The blue-shift of the principal emission component observed in some events at flare onset has been interpreted in

Section 4.3.1.3 as due to chromospheric material that was evaporated at low velocity in the confinement region. This interpretation is not corroborated by the same large set of data available for the high speed upflows. However, if this is the case, at this stage only moving, evaporated material is observed, since the coronal region is still at low density, permitting a direct estimate of the conditions of the moving SXR source.

Considering the May 21 event at the time of the first calcium emission (first spectrum in Figure 4.2), an upflow density of about 3×10^{10} cm^{-3} is derived by inferring the volume from the HXIS SXR images in Figure 4.3. Considering that the temperature of the moving evaporated material is 9×10^6 K, that its turbulent velocity is 220 km s^{-1}, and that its bulk velocity is 80 km s^{-1}, the rate of enthalpy, turbulent, and kinetic energy input into the loop through the footpoints is about 2×10^{27} ergs s^{-1}. The enthalpy and turbulent energy inputs are the most significant. The energy input rate to the coronal region due to the low-speed upflow is comparable with the energy input to the chromosphere associated with the electrons accelerated to energies of about 25 keV entering the thick target region.

The density and temperature derived for the slowly moving material do not differ much from the values indirectly derived for the high speed upflows, observed later on. The mass and energy input of this component to the corona at this stage is however negligible, as pointed out earlier.

4.3.1.7 Energy Input into the Chromosphere During Evaporation

The energy input into the chromosphere during the evaporation process can be derived easily under the hypothesis of thick target interactions by non-thermal electrons. This quantity can be computed from the HXR spectra measured with the Hard X-ray Burst Spectrometer (HXRBS), assuming a power-law electron spectrum with a cutoff at 25 keV. It is found that for the flares of Table 4.1, the rate of energy input by energetic electrons is sufficient to account for the increase in the thermal energy of the SXR emitting coronal plasma at all times during the impulsive phase. The total increase of coronal energy during the evaporation process ΔE_{SXR} is compared with the total energy input by non-thermal electrons ΔE_{HXR} in Table 4.2. The energy input cannot obviously be directly compared with the energy transferred by the upflows to the corona since this quantity has been derived under the requirement that it match the increase in coronal energy during the impulsive phase (Antonucci, Gabriel, and Dennis 1984). For the June 6, 1982 event, discussed by Tanaka, Ohki, and Zirin (1985), it is also found that the HXR emission implied a chromospheric energy input sufficient to account for the large conduction losses and the increase in thermal energy of the flare.

Hence, at least for the case of non-thermal electrons injected into the chromosphere, the HXR flux can be an indicator of an energy deposition indeed sufficient to account for the increase of coronal plasma energy content, while the upflows, under the conditions mentioned before, can provide the appropriate energy transfer mechanism.

The total energy ΔE_{tot} radiated and conducted away during these flares is also given in Table 4.2. From these values it appears that no energy input is in general required after the upflows are no longer observed.

4.3.1.8 Conclusions

The SMM data have allowed us to derive the general properties of the upflows of high temperature plasma observed during the rise of solar flares and to localize, in few cases, their sources in the flare region. From these results we can conclude that the plasma rising into the corona is indeed the primary source of the thermal plasma observed in the corona during flares. This conclusion is not only supported by qualitative considerations, but also by quantitative tests on mass and energy balance during the impulsive phase. Within the present observational limitations, the conditions required for plasma upflows to account for the flare coronal plasma are consistent with the observations.

The most natural mechanism we can invoke to explain the origin of such plasma upflows is indeed chromospheric evaporation. This process is in fact predicted in any simulation of impulsively heated coronal loops. We note however that even in the alternative model proposed by the con team, for instance, upflows are still needed to supply most of the plasma contained in some of the magnetic configurations which brighten during a flare, although their origin in this case is of a different nature.

Since the quantitative tests presented here as supporting evidence for the main role of upflows in the formation of the flare coronal plasma are very important in our discussion, and since they are influenced more than other results by the present instrumental limitations (which do not allow, for instance, a direct measurement of the electron density of the blue-shifted component, or knowledge of the detailed topology of the magnetic configuration and its time evolution), it is worthwhile to stress a few points. For the events we have analyzed, a pressure difference sufficient to drive upflows into the coronal region where they are confined is easily obtained for values of the flare region volume compatible with the observations. Solving the continuity equations, the electron temperature of the upflows is found to be of the same order as that obtained for the coronal source. Its value, in fact, cannot be much lower otherwise the blue-shifted satellite lines due to dielectronic recombination would significantly increase and therefore they would be resolved and observed. Moreover, at least for a set of flare volumes considered in our discussion, the lower limit of the electron density of the upflows is of the same order as the density of the coronal loop at the end of the accumulation process, thereby exceeding the coronal density during evaporation.

Therefore, the pressure of the upflows can be considered larger than the pressure in the loop at any time.

The emission measure of the stationary component varies according to the plasma input rate in the flaring loops, which is regulated by the electron density of the blue-shifted component and its velocity. The electron density is indirectly derived from the emission measure of the blue-shifted component which is also related to the volume where the plasma is propagating. Except at flare onset, the propagation region in a closed configuration represents only a part of the flux tube, since the rest of the loop is filled by stationary plasma whose emission is increasing as a flare progresses. For the flare volumes that satisfy the pressure requirement for plasma flows into the coronal loop, the effective volume occupied by upflows is found to be about 20% of the total volume. This value is averaged over the impulsive phase. The region where upflows are confined is presumably near the base of the flux tube. At flare onset, we can infer that the volume where upflows propagate is close to the total volume of the confining region.

There is evidence to suggest that the process of mass transfer to the corona often begins at low velocities. This is the phase when the blue-shifted component is observed to be dominant, while the stationary source is either weaker or absent. However, this phase is difficult to study since the blue-shift corresponds to low velocities and line-of-sight effects become important for its detection. In the few cases where this effect is well observed, the hard X-ray emission begins with low intensity, prior to the impulsive bursts. We can therefore deduce that coronal loops are first filled by low velocity plasma flows induced by a moderate chromospheric heating; the high velocity upflows only appear after the energy release becomes impulsive. In our opinion, a more accurate profile of the heating function accounting for a slow initial rise should be applied to coronal loops in the numerical simulations. This may be an important factor in determining the actual physical conditions of a coronal loop at the time of the major impulsive energy release.

4.3.2 Argument Against: The Blue-shifts Are Direct Evidence of Chromospheric Evaporation

The arguments against the blue-shift and chromospheric evaporation connection are based mainly on three observational properties of the X-ray and UV spectral lines. First, there are no instances in which a large blue-shifted component is the only component present during the rise phase. Second, some spectral lines should not show both blue-shifted and stationary components, but instead should show only a blue-shifted component. This is not found for one such well-observed line, the Fe XXI line at 1354.1 Å. Third, the electron density of the SXR flare is apparently high at flare onset, and therefore not as much chromospheric evaporation is necessary as has been previously assumed. However, this argument is not as strong as the first two mentioned. Below these arguments are discussed more fully.

4.3.2.1 Relative Intensities of Blue-shifted and Stationary Components of X-ray Lines

If the high density of SXR flares is primarily due to evaporating plasma from the chromosphere, then at some early time during the rise phase the large blue-shifted component should be the dominant spectral feature. The stationary component should be much weaker than the blue-shifted component or nonexistent. This is not observed in available flare spectra. The stationary component is always at least as strong as the blue-shifted component, implying an already existing high density loop, and contradicting predictions based on numerical simulation models.

The relationship between blue-shifted and stationary components has been made quantitative by Doschek *et al.* (1983) and Cheng, Karpen, and Doschek (1984), who discuss the shapes and Doppler shifts of spectral lines in terms of the gasdynamics of evaporation. The Doschek *et al.* (1983) paper discusses a flux tube that is heated in a localized region at the top of the loop. The conservation equations of mass, momentum, and energy are solved numerically for a two fluid plasma consisting of electrons and protons. The heating is symmetric, that is both sides of the loop receive the same amount of flare energy. A conduction front rushes down both sides of the loop and eventually drives chromospheric evaporation. (We note that actually only a half-loop was simulated in this calculation; see Cheng *et al.* (1983). There are some possible differences between a half loop and a full loop simulation but these are of no consequence to our arguments.) The effects on spectral lines of evaporation for the special case of a symmetrically heated loop have been predicted by Doschek *et al.* (1983) and are summarized below according to temperature of line formation. The maximum temperature reached in the loop is about 20×10^6 K, at the top of the loop. Although the Doschek *et al.* (1983) results represent only a restricted range of possible input parameters, we believe that similar results should be obtained for a rather wide range of input parameters, assuming symmetric heating. Also, we note that chromospheric heating by electron beam simulations generally give evaporation velocities much larger than the observed blue-shifted velocities (Fisher, Canfield, and McClymont 1984). Thus, we restrict the simulation discussions to conduction heating models, because at least they give evaporation velocities that are comparable to the observed blue-shifted velocities.

Chromospheric and transition region lines ($T < 10^6$ K). These lines should show small red-shifts on the order of 20 km s^{-1}. The chromosphere and transition region are driven inward by evaporation. Because of their relatively high densities the inward velocities are small. The lower density evaporating plasma has been heated by conduction to temperatures

of several million degrees and evaporates with much higher velocities.

Coronal lines (10^6 K < T < 3 × 10^6 K). These lines are predicted to show essentially no Doppler shift (when viewed at Sun center). Gas at temperatures of one or two million degrees is at the dividing region between upward evaporating plasma and downward moving chromospheric and transition region plasma.

Low temperature flare lines (3 × 10^6 K < T < 10 × 10^6 K). Spectral lines formed between about 3 and 10 × 10^6 K should show only a blue-shifted component, as long as evaporation persists. These lines are formed in the region that is evaporating with a large range of velocities. For a line formed near 10 × 10^6 K, the upward velocities range between 200 and 400 km s^{-1}. For a cooler line formed near 5 × 10^6 K, the upward velocities would be less, but still no stationary component should be present.

High temperature flare lines (T > 10 × 10^6 K). These lines should show a blue-shifted as well as a stationary component. The stationary component arises from gas at the top of the loop where the temperature is highest. The abundances of high temperature ions are largest at the highest temperatures, and the contribution functions of the high temperature spectral lines are further increased at high temperature by the Boltzmann factor in their excitation rate coefficients. However, the density at the top of the loop is initially quite low compared to the density of the evaporating plasma, and the intensity of these lines is proportional to N_e^2. Thus the relative intensities of the blue-shifted and stationary components of high temperature lines at any given time during evaporation depend on the temperature, density, and velocity distribution of the gas within the loop. The results of the simulation show that during the initial stages of evaporation, the blue-shifted component should be dominant. As evaporation proceeds, the ratio of the blue-shifted to stationary component decreases, and eventually the stationary component dominates.

The arguments concerning the high temperature lines given above cannot be rigorous because of the difficulty of including time-dependent ionization calculations in the simulations. That is, the Doschek *et al.* (1983) paper assumes ionization equilibrium in the calculation of line intensities and profiles. This assumption is not valid for times less than about 20 s in the Doschek *et al.* simulation. However, the effect of time-dependent ionization is strongest on the stationary component, because it has the lowest density. Qualitatively, the effect of including time-dependent ionization would therefore appear to be to reduce the ratio of the stationary to blue-shifted component, at least in some cases. Examples of computed profiles in this symmetric calculation are shown in Figure 4.4.

The description of line profiles and shifts given above might be modified if the loop size in the Doschek *et al.* (1983) simulations were greatly lengthened. However, the results are substantially modified if the heating is asymmetric, that is, if most of the flare energy is put into one side of the loop. In the Cheng, Karpen, and Doschek (1984) simulation of this situation, evaporation proceeds up both legs of a loop, but evaporation from the heated side of the loop is strongest. This results eventually in a net flow of plasma up the leg of the heated side of the loop and down the other leg.

The net flow of plasma within the loop has a dramatic effect on the line profiles. For cool flare lines formed between ≃ 3 and 10 × 10^6 K, the profile is split into both a blue-shifted and red-shifted profile. For the hottest flare lines there is blue-shifted and red-shifted emission, as well as emission at the rest wavelength. Examples of profiles from asymmetrically heated loops are shown in Figure 4.5.

A comparison of the numerical simulation results discussed above with observation reveals several disturbing discrepancies. For one, the observed blue-shifted component of the Ca XIX resonance line is much less intense relative to the stationary component, in contrast to what is predicted by the simulations for early rise times. The onset times of the flares in the P78-1 data base can be estimated to within seconds from noting when the proportional counter broadband X-ray data (also from P78-1) first show an increase in count rate. Another method of estimating onset time is to fit the early rise with an exponential (see Feldman, Doschek, and McKenzie 1984). The flux predicted from the exponential can then be extrapolated back in time and an approximate onset time can be determined. It is possible by measuring the angular steps at which the peak line emission occurs during the course of a flare to determine if the wavelength of peak emission changes with time. For the flares observed with P78-1, the wavelength of peak line emission appears to be nearly constant. It is clear that a strong, and in fact, usually totally dominant, stationary component is present within 10 s of the onset times of the flares.

Another disturbing aspect of the observed blue-shifted X-ray line components arises because they are seen not only in flares with relatively short rise times, i.e., < 2 minutes, but also in flares with very long rise times. An outstanding example is the June 5, 1979 flare (see Doschek *et al.*, 1980). In this flare, which had a rise time of about 30 minutes, the blue-shifted component is present during the rise phase indicating about the same velocity (≃ 300 km s^{-1}) as found for more impulsive flares. In general for the X flares, the upward velocities indicated by the blue-shifts are *much larger* than necessary to account for the observed EM increase. Velocities less than 10 km s^{-1} are needed in some cases, so even if chromospheric evaporation occurs, there is a mismatch between the observed blue-shift velocities and the required chromospheric evaporation velocities. Note also that the intensity of the blue-shifted component for most flares is at all times much less than the intensity of the stationary component. (The ratio is about 0.2). The cases where the intensity ratio is larger, such as with the two M flares reported by Feldman *et al.* (1980), are exceptional.

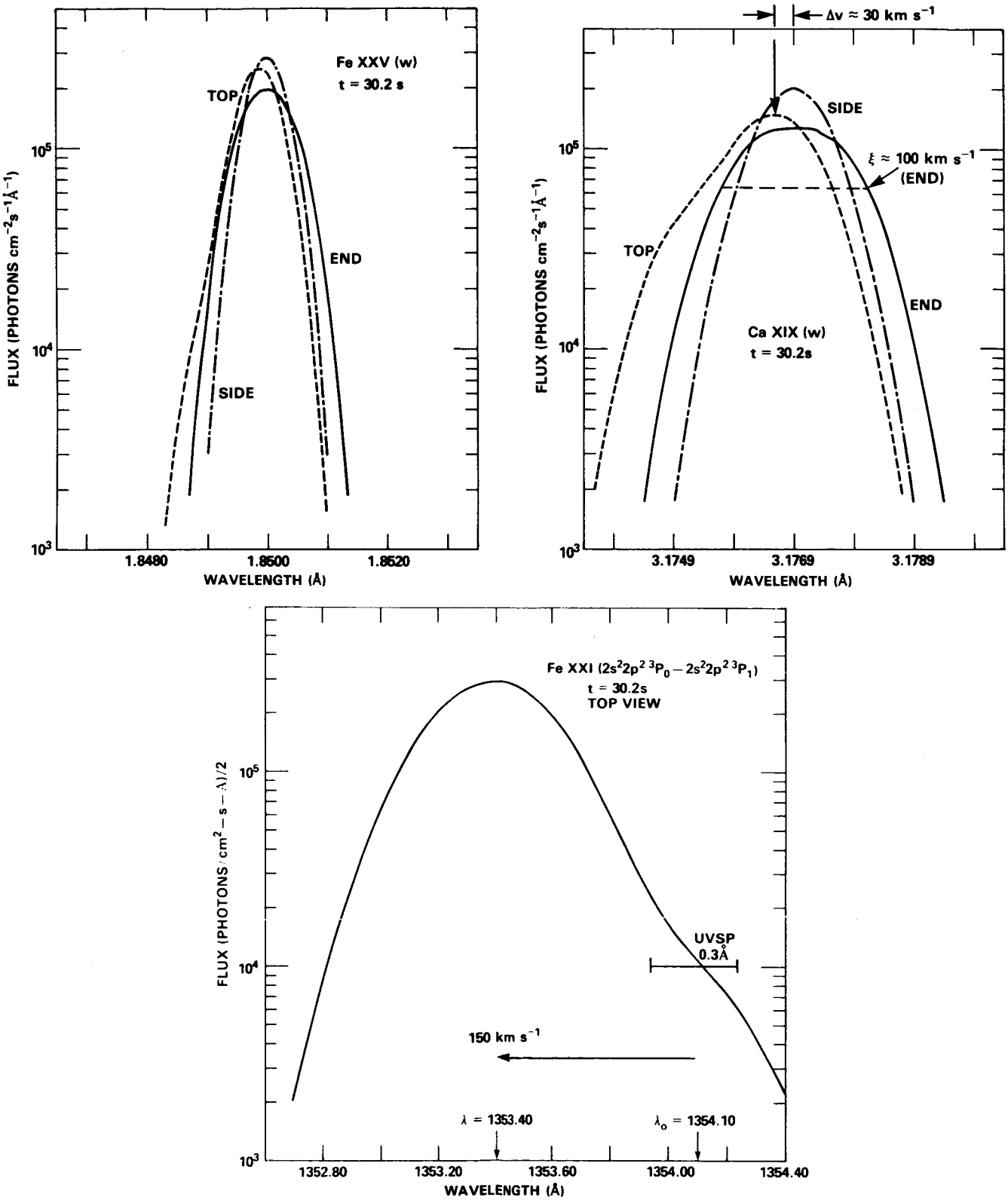

Figure 4.4 Computed line profiles of the resonance lines of Ca XIX, Fe XXV, and the forbidden line of Fe XXI at about 30 s after onset of flare heating in a loop heated at the top. Various line-of-sight viewing angles are shown. The half-length of the loop was 6700 km and the initial pre-flare loop density was 6×10^9 cm^{-3} at the loop top. See Cheng *et al.* (1983) and Doschek *et al.* (1983) for details.

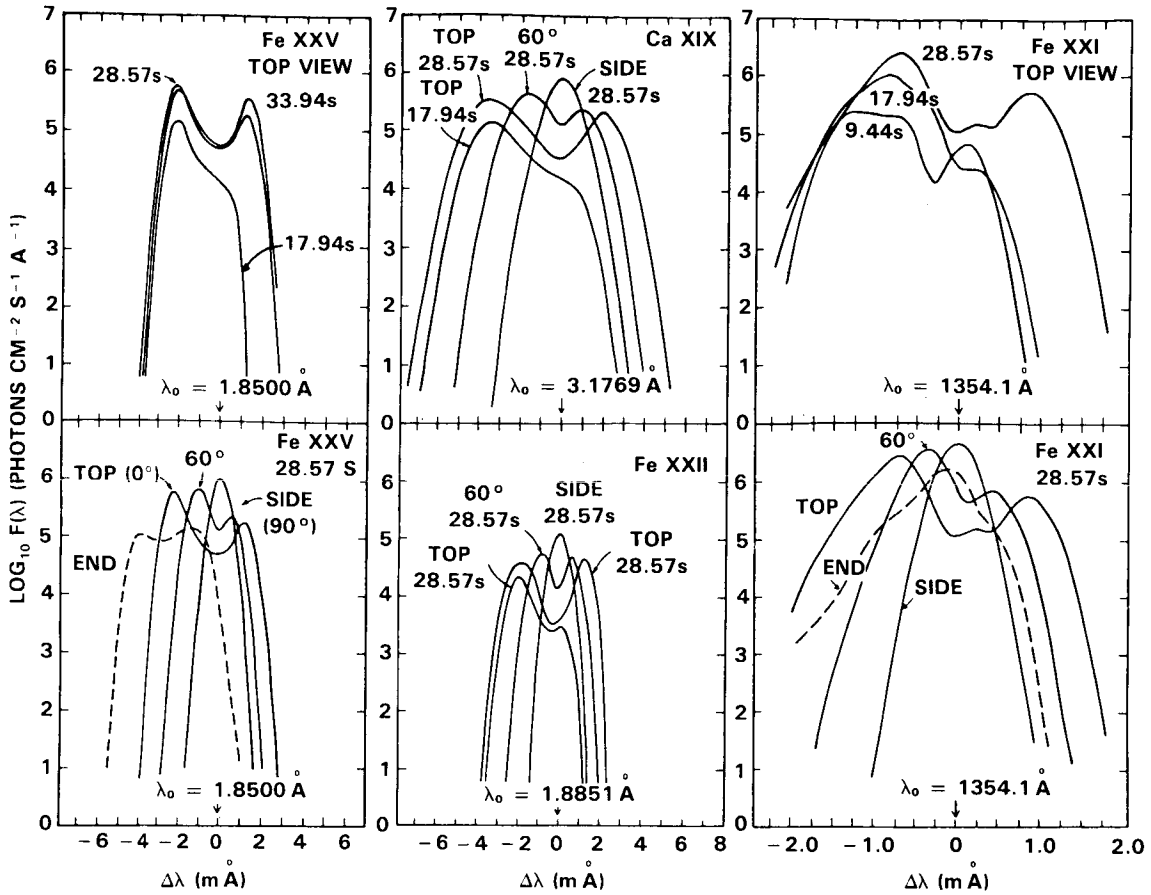

Figure 4.5 Computed line profiles of the lines shown for the asymmetric heating calculation described in the text. The profiles are shown at about 28 s after onset of flare heating. See Cheng, Karpen, and Doschek (1984) for details.

To make the above remarks quantitative, consider a loop model that is qualitatively the same as adopted by the pro team in their attempts to support the evaporation theory. The model is modified by assuming for simplicity that the density of the evaporating plasma n_e' is essentially the same as the density in the loop. This is a rough prediction of the simulations discussed above and is also consistent with the observations and analysis used by the pro team. The rate of change of total number of electrons in the loop is,

$$\frac{d(n_e V)}{dt} = 2n_e' A v', \qquad (1)$$

where v' is the upflow velocity, V is the assumed constant loop volume (= LA, L=loop length), A is the cross-sectional loop area, and the factor of 2 accounts for both loop footpoints. The emission measure $EM = n_e^2 V$, or

$$\frac{d(EM)}{dt} = 2n_e V \frac{dn_e}{dt} \qquad (2)$$

Assuming as mentioned for simplicity that $n_e' = n_e$,

$$\frac{d(EM)}{dt} = 4n_e^2 AL\, v'/L \ , \qquad (3)$$

or,

$$\frac{d(EM)}{dt} = 4(EM)\, v'/L \ . \qquad (4)$$

Finally,

$$(EM) = (EM)_o \exp(4\, v't/L) \ . \qquad (5)$$

In order to explain the June 5, 1979 EM increase as due to evaporation at the speed of about 300 km s^{-1} indicated by the observed blue-shifts, equation (5), the rise time of about 30 minutes, and the ratio $(EM)/(EM)_o = 200$ observed over the 30 minute interval, show that $L \simeq 4.1 \times 10^5$ km or 9.4 arcmin. Such a length is improbably large. The problem can be circumvented by assuming the existence of several loops, such that V is not constant with time. However, in this case it is difficult to significantly increase the density in each loop,

since multiple loops are needed to continuously increase V. Although in fact flares are usually composed of several loops, this discussion shows that the single loop chromospheric evaporation model does not account for all the observations.

We note that equations (1-5) also implicitly assume that n_e is constant in the loop, which is not a good assumption. However, in our simulations, n_e usually increases monotonically with decreasing temperature, and $n_e' > n_e$. The effect of a varying electron density can be approximated by assuming that $n_e' = \beta n_e$, where $\beta \gtrsim 1$. In this case the term $4v't/L$ in equation (5) becomes $4\beta^2 v't/L$. Since $\beta > 1$, the length of the 5 June flare loop inferred above would have to be even larger for a fixed value of EM/EM_0 and a heating time of 30 minutes.

Finally, if flare loops are really heated asymmetrically, then the X-ray observations are at even greater variance with the predictions of the numerical simulations. There are only a few cases where red-shifted components of X-ray lines are seen, and these are confined to limb events (e.g., Kreplin, *et al.*, 1985). On the other hand, there is ample evidence that real flare loops at least appear asymmetric in the brightness distribution of X-ray and EUV emission (e.g., Pallavicini, Serio, and Vaiana 1977).

4.3.2.2 Lack of Blue-shifts of Cool Flare Lines

Observations of cool flare lines ($6 \times 10^6 < T < 10^6$ K) are available from the NRL Skylab spectrograms and spectroheliograms, and from the UVSP SMM experiment. The Skylab spectoheliograph observed in the range from about 170 to 650 Å. It formed monochromatic images of the flare plasma. The predicted upflow velocities for chromospheric evaporation are between 200 and 400 km s^{-1}. As noted, the observed blue-shifted X-ray line component also implies velocities of about 300 km s^{-1}. At a wavelength of 200 Å these velocities correspond to Doppler shifts of between 0.2 and 0.4 Å. These shifts are easily measurable on the Skylab spectroheliograms, for which the resolution is high enough to measure shifts of a few hundredths of an Angstrom. However, there are three difficulties with the spectroheliogram data. First, very few large flares were observed from Skylab since the experiment was performed near solar minimum. Second, the time resolution of the instrument was poor and only one or two events were actually observed during flare rise time.

Finally, since the slitless instrument forms images, a Doppler shift can be interpreted as a spatial shift, and vice-versa. Flares are frequently composed of more than one loop, and so it becomes very difficult to unambiguously separate Doppler and spatial shifts. The situation is well illustrated by the analyses of the 15 June 1973 flare presented by Cheng (1977) and Widing and Dere (1977). The images of the flare shown in those papers are quite complicated (even though the 15 June event had a typical SXR light curve), and at least two loop systems were involved. In spite of the caveats mentioned above, it was possible for Widing (1975) and Brueckner (1976) to identify blue-shifted emission features in the 15 June flare. In particular, the so-called "spike" (blue-shifted emission feature) is clearly a Doppler shifted feature (see Figure 4.6). However, this blue-shifted feature emanates from the *top* of the loop systems, rather than from the footpoints, and it shows up over a broad range of temperatures. The emission is observed in lines of He II, Fe XV, Fe XVI, and possibly Fe XXIV. The emission is observed in one rise phase spectrum (the only such spectrum available) and in two or three spectra obtained near maximum X-ray flux. This shows that at least some blue-shifted emission can arise from regions other than footpoints, and provides a counter example suggesting that the origin of the blue-shifts for at least some flares is located near the tops or sides of loops, rather than at their footpoints. In addition to the blue-shifted "spike" emission, the centroid of the Fe XXIV emission shifts about $5''$ from NW to SE in about four minutes around the time of peak X-ray flux. Widing and Dere (1977) suggest that another loop system may be activated. These observations simply point out the extreme geometric complexity of real flares. Very high spatial resolution is needed to distinguish small spatial shifts such as we are discussing. The spatial resolution of the Skylab spectroheliograph was $2''$.

The complexity of flares as seen with high spatial resolution implies that it is very difficult, if not impossible, to unambiguously identify individual footpoints of loops with the instruments on SMM and Hinotori. The spatial resolution of these instruments is at least a factor of 5 less than the Skylab instrument. Thus, the pro team arguments revolving around the locations of SXR and HXR emission, and analyses such as given by Antonucci *et al.* (1982) that depend significantly on knowledge of the SXR emitting volume, are inconclusive. They demonstrate only consistency with the evaporation model, and this consistency is made possible because the SXR volume is poorly known and the spatial resolution is coarse enough to be consistent with a proposed relationship even if the relationship does not in fact exist.

Finally, Acton *et al.* (1982) and the pro team argue that chromospheric evaporation was reported in the analysis of Skylab spectroheliograph data by Hiei and Widing (1979). This is true, but a close inspection of their paper reveals that the supposed evaporation does not occur in the loop or loops responsible for most of the Fe XXIV emission. It is these loops that would give rise to the high temperature X-ray lines presently under discussion. The loop discussed by Hiei and Widing (1979) was a cool loop with a temperature no more than 6×10^6 K. Furthermore, a further analysis of the same flare by Widing and Hiei (1984) shows that at least one location of HXR and XUV emission from this flare is physically completely separated from the loop or loops in which the SXR emission arises.

Another cool flare line observed from Skylab is the Fe XXI forbidden line, due to the magnetic dipole transition,

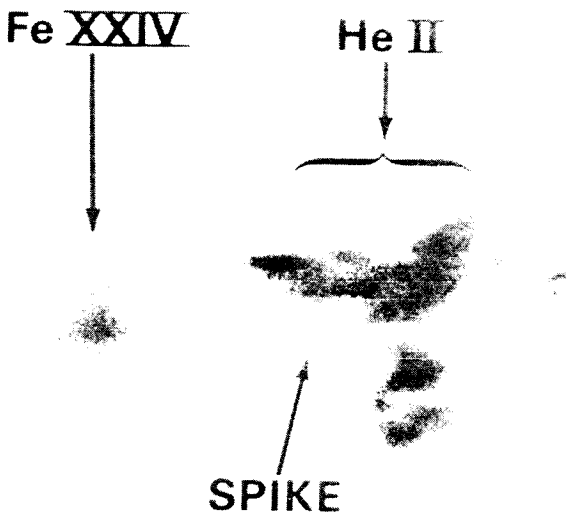

Figure 4.6 An NRL S082-A Skylab spectroheliogram of the June 15, 1973 flare showing images of the flare in Fe XXIV (255.1 Å) and He II (256.3 Å). The feature marked "spike" is blue-shifted He II emission. The blue-shift corresponds to a speed of about 400 km s^{-1}. This feature is also apparent in lines of Fe XVI and Fe XV. Note that a superposition of the He II and Fe XXIV emission shows that the "spike" arises from the top of the loop system, rather than from the footpoints.

$2p^2\ ^3P_1 -> 2p^2\ ^3P_0$, at 1354.1 Å. This line was identified independently by Jordan (1975) and Doschek *et al.* (1975). The line was observed with the NRL slit spectrograph, which had a resolution of 0.06 Å. Because the line is formed at about 8×10^6 K, and the flare plasma is turbulent, the line is quite broad and near X-ray maximum it can have a FWHM of about 0.5 Å.

Fe XXI data were obtained for a number of flares observed during the Skylab mission (e.g., Cheng, Feldman, and Doschek 1979). Recall from the previous discussion that for a line formed at 8×10^6 K, no stationary component should be present. Furthermore, at this temperature a spectral line such as the Fe XXI line should be shifted for as long as evaporation occurs. Even though not many flares were recorded during the rise phase, there were at least some spectra recorded during this phase and in any event the emission measure (and therefore presumably evaporation) frequently continues to increase somewhat after the peak X-ray flux is reached. Therefore, it is expected that the centroid wavelength of the Fe XXI line should vary considerably in different spectra. But this was not found to be the case. The wavelength of the Fe XXI line in all the spectra does not vary by more than about 0.02 Å, or equivalently, about 4.5 km s^{-1}. This result is in contradiction to what is expected from the evaporation model.

More recently, Fe XXI data have been obtained from the SMM UVSP instrument (Mason *et al.*, 1985). They report blue-shifted components of the Fe XXI line in some of these data. However, a strong stationary component appears in all cases and the blue-shifted component velocity is much smaller than expected from the numerical simulations. Also, as Jordan (1985) has noted, there are several chromospheric lines in the region around the Fe XXI line, and care must therefore be exercised in interpreting possible blue or red wings to the Fe XXI line. Mason *et al.* (1985) have taken this into account in their analysis, however.

4.3.2.3 High Preflare Electron Densities

In the chromospheric evaporation picture, the high electron density of a flare is produced mainly by the large upward mass flux from the chromosphere. In this scenario the loop before flare onset is usually assumed to have a relatively low electron density, say considerably less than 10^{10} cm^{-3} (Nagai 1980). That is, if the initial loop density is much higher, there is no need to invoke evaporation to explain the large mass in the corona; it is there to begin with. Typical SXR flare densities at flare maximum have been estimated by different investigators to be between about 10^{11} and 10^{13} cm^{-3}. However, most values fall between 1 and

5×10^{11} cm^{-3}. If the initial loop density were also high, then in this case a large mass is already present at high altitudes, and chromospheric evaporation may not be the dominant or only mechanism that produces the high SXR flare density.

It is important to mention how the electron densities are measured. For temperatures less than or comparable to 6×10^6 K, densities can be derived from density sensitive spectral line ratios (e.g., Dere *et al.*, 1979). Densities obtained from a number of different ratios all give values on the order of 10^{11} cm^{-3} or greater. For temperatures greater than 6×10^6K, there are not adequate spectral line ratios. However from Skylab, P78-1, and SMM, there are images of flares in high temperature spectral lines, such as Fe XXIV 225 Å in the Skylab data. The Skylab data have the highest spatial resolution, about 2″. From the incident flux in the image the emission measure n_e^2 V, can be derived. Then the volume V can be calculated from the image and plausible geometric assumptions about the shape of the flare. Thus, the electron density n_e can be calculated. This method also gives densities greater than 10^{11} cm^{-3} for the SXR flare. Finally, Feldman, Doschek, and Kreplin (1982) estimated electron densities greater than 10^{12} cm^{-3} for very impulsive flares that cool in a minute or so. This estimate results from the very short cooling times and large emission measures. The high density is obtained whether or not the cooling is due to conduction or to radiation. In summary, all evidence points to very high densities for SXR flares at times near peak SXR emission.

Measuring densities at flare onset times is much more difficult because X-ray fluxes are very low and high time resolution is needed. The best way at present to infer onset time densities involves neither a density sensitive line ratio nor an X-ray image. Instead, an attempt is made to use the fact that it takes a finite time after heating a plasma to strip the heavy elements to He-like and H-like ionization stages, i.e., to reach ionization equilibrium (IE). As explained in Gabriel (1972) and Doschek, Feldman, and Cowan (1981), it is possible to use combinations of line ratios to measure the departure from IE.

Figure 4.7 shows the IE line ratio diagnostic q/w and the abundances of He-like calcium and iron compared to the total element abundance as a function of the parameter $n_e t$, under the assumption of instantaneous heating of plasma from $1 - 2 \times 10^6$ K up to the values shown in the figure. That is, the time dependent rate equations for ionization and recombination were solved as a function of time assuming a step increase in temperature (and also a constant density). The procedure is described by Doschek (1984). The relevant parameter is $n_e t$, and not simply n_e or t.

These curves are to be understood as follows. The fractional abundance N(Ca XIX)/N_T and ratio q/w have values of 0.43 and 0.71 respectively, for $n_e t = 10^{11}$ cm^{-3}s. That is, if $n_e = 10^{11}$ cm^{-3}, then these values will be reached in

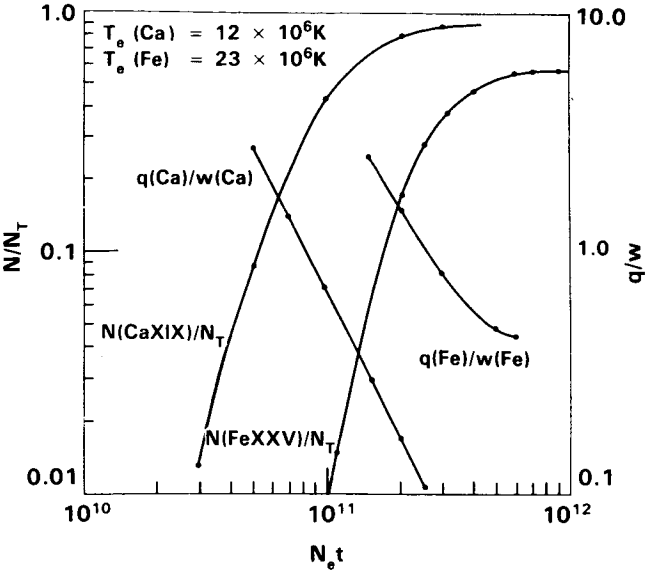

Figure 4.7 Transient ionization calculations for calcium and iron. The calculations assume calcium and iron ions are heated instantaneously from temperatures of 1-3 × 10^6 K to temperatures of 12 × 10^6 K and 23 × 10^6 K, respectively. The fractional He-like ion abundances and the key diagnostic ratio q/w are shown. The equilibrium ratio of q/w for calcium is about 0.09 in this calculation.

a time of 1s. If $n_e = 10^{10}$ cm^{-3}, then these values are achieved in 10s, and so forth. From inspection of these curves, it would be difficult to measure a departure from IE using q/w ratios for $n_e t = 2 \times 10^{11}$ cm^{-3}s for calcium and perhaps 3.5×10^{11} cm^{-3}s for iron. Thus for $n_e = 10^{11}$ cm^{-3}, a time resolution better than about 3.5s is needed to detect departures from IE. However, for $n_e = 10^{10}$ cm^{-3}, departures could be observed in times of about 10 - 20s after flare onset.

Up to now, the earliest spectra observed during the rise phase either with P78-1 or SMM appear to be consistent with IE. Therefore it must be concluded that for most if not all flares the preflare loop density is at least 10^{10} cm^{-3}. It might be argued that in the evaporation theory this is not unexpected since plasma at transition region and chromospheric densities is being heated. Nevertheless, a strong stationary component of X-ray spectral lines is already present 10 - 20s after flare onset, and this must represent plasma already evaporated or initially present in loops. For impulsive flares, as opposed to the slow rise phase flare discussed earlier, the evaporation velocity needed to fill the loops in 10 - 20s is much larger than the velocity indicated by the blue-shifted component, and is not consistent with the evaporation scenario.

The conclusion is that the stationary component of X-ray spectral lines represents a high density plasma with $n_e > 10^{10}$ cm^{-3}, even at flare onset. It should be emphasized that

this density is a lower limit. Observations within 10s of SXR flare onset are hampered by low counting rates and other instrumental problems.

In summary, a careful comparison of available X-ray data with predictions from numerical simulations of chromospheric evaporation reveal several striking discrepancies. The con team does not believe that these discrepancies can be resolved by either better data or a more adequate theory that for example would fully resolve the flare transition region. After all, the basic result of the simulations is the self-evident one that plasma flows upward into loops at about the sound speed, a result that can be qualitatively derived very simply. The upflowing plasma must be hot if it is heated in the conventional manner, i.e., either by conduction or beams. In this case some X-ray or EUV lines should show strong blue-shifts *for the bulk of the emission*, and this is not observed. Although the data base could certainly be improved upon, the con team takes the position that it is adequate to demonstrate the discrepancy. Finally, it would still be possible to have the mass of the SXR plasma supplied from the chromosphere without contradicting the X-ray observations if it is hypothesized that the chromospheric plasma is lifted into the corona by magnetic forces, similar perhaps to the eruption of a prominence (Pallavicini, Serio, and Vaiana 1977, Moore *et al.*, 1980). In this case the plasma would be cold while lifted into the corona, and then heated after large upflow velocities cease. Such a view has been suggested by Hudson (1983). However, the con team remarks that the physics of this process is entirely different than the physics of the "popular" evaporation scenario under discussion. Hudson's (1983) suggestion represents a major departure from the prevailing view of how chromospheric evaporation occurs, and is beyond the scope of this debate.

4.3.2.4 An Alternative Multiple Loop Model

If chromospheric evaporation does not account for the high densities of soft X-ray flare plasma, then how are such high densities achieved? Furthermore, since blue wings *are* observed on the wings of X-ray lines during the rise phase, another origin for them must be found if the chromospheric evaporation explanation is not accepted. The con team felt somewhat obligated to provide an alternative model that would account for all the observations, although strictly from the point of view of the debate this was not necessary.

The con team adopts the viewpoint that *some* of the blue-shifted material could be due to chromospheric evaporation, or ablation, but that this process is not the main cause of the high densities in soft X-ray flare plasmas. It is possible to envisage a rather different alternative model to that proposed by the pro team. In their model, the flare *takes place* within a single loop, although the *energy* to cause the flare is often considered to arise through magnetic field reconnection with another loop. In the model proposed below not only energy transfer, but mass transfer takes place during the reconnection process. This concept has, of course, been proposed previously in the context of high energy electrons leaking onto field lines above the original flaring region, causing for example radio emission. But the transfer of substantial amounts of mass during the impulsive phase has not been previously stressed. The concept is a natural consequence of the reconnection of two loops which have substantial helical components to their fields, in the same sense. The "reconnected" field would envelope both previous loops (see Figure 4.8).

Many authors have discussed flares observed both during the Skylab missions and SMM in terms of multiple loops. There is also a long history of flare models involving more than one loop and flare heating by magnetic energy dissipation or field line reconnection. Thus it seems natural to consider how the blue-shifted component could arise in these circumstances.

Consider a set of loops such that the large loops have a lower temperature and density. This is known to be the situation in loops associated with active regions (e.g., Gabriel and Jordan 1975). The emerging flux model as discussed by Heyvaerts, Priest, and Rust (1977) also gives a useful framework. With the emergence of new flux the pre-existing field configuration will be disturbed. This is observed through filament activation and disappearance. As part of this re-arrangement either the newly emerged flux *or* overlying flux loops may reach a configuration where reconnection can occur. The reconnection process will cause particle acceleration and plasma heating. It is unlikely that the pressure in the two loops (or more) will be identical. The reconnection will bring particles from the denser loop onto the field lines of the less dense loop(s) during the impulsive phase. The pressure difference could cause a net upflow of particles, unless the reconnection takes place very close to the loop apex. Thus, the observed blue-shifts could result from "injected" material rather than ablated plasma. In addition, particles accelerated during the reconnection phase can penetrate to the loop chromospheres giving rise to hard X-rays. Particles in the lower density loop will be able to reach the more distant footpoint in a non-symmetric situation. Heating of both the denser and less-dense loops will no doubt occur. In general the dramatic dynamic effects might be expected to occur in the less dense loops. The main soft X-ray emission could in principle arise from the accumulation of injected plasma, but clearly a range of flare behavior could result, depending on initial parameters and geometries. For example, the dense reconnecting loop when heated further through reconnection could also give rise to increased emission. This dense loop might have field lines that strongly and rapidly converge near the chromosphere, or conduction might be inhibited by anomalous effects. Therefore evaporation into the initially dense loop could be insignificant. Observations of this loop would reveal an initially dense loop with unshifted spectral lines, thus explaining the origin of high densities without invoking large Doppler shifts.

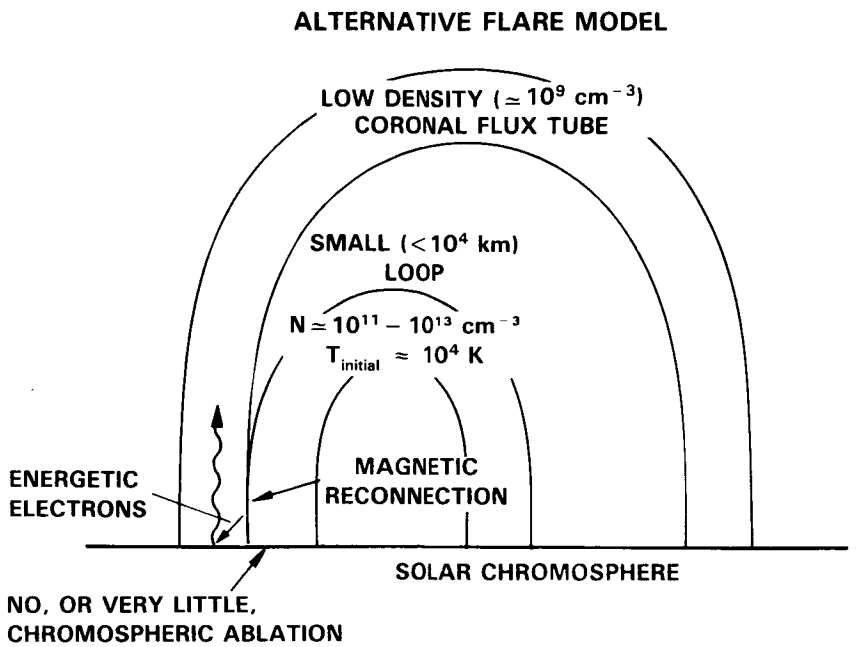

Figure 4.8 A possible alternate flare model that would produce blue-shifted components on X-ray emission lines while always maintaining a strong stationary component. Note that the proposed reconnection involves the *poloidal* components (not shown) of the magnetic fields defining each loop.

The sequence of events described by, for example, Feldman, Doschek, and Rosenberg (1977) and Doschek, Feldman, and Rosenberg (1977) for the June 15, 1973 flare, or by Dere and Cook (1979, 1983) and Dere *et al.* (1979) for the August 9, 1973 flare, finds a natural explanation in a multi-loop model, as indeed some of these authors discuss. Pressures that are higher in the hot regions than in the cool regions can be accounted for by the relative emission measures of different loops.

Whether or not the material is evaporated or injected, the time dependence of the blue wing flux can be examined to see whether or not it could "become" the static component — in this model arising from the "filled" portion of the loop. However, as pointed out by the pro team, there are no sufficient observations available to test this hypothesis. In particular, the temperature of the blue wing material is an important parameter which has not been measured. Studies of the blue wing asymmetry simultaneously over a range of coronal ions (O VII - Fe XXV) and in the transition region are urgently required.

Acton *et al.* (1982) computed total XRP band emission measures and compared these quantities with evaporation indicated by Hα analyses but not with any blue-shifted component in X-rays. Their pressure difference between the Hα and X-ray regions finds a natural explanation in a multi-loop model (see below). However, a re-examination of the Hα modelling removed this discrepancy (Canfield and Gunkler 1985). In a later paper Gunkler *et al.* (1984) summed the blue-wing emission measure and claimed agreement with the static component but they do not discuss the relative temperature or densities of the two components. Thus although there is evidence that the amounts of material emitting in X-rays is within an order of magnitude of that "evaporated", the hypothesis of identity must still be regarded as "not proven".

In summary, the con team regards the evaporation explanation of blue-shifted X-ray lines as inconclusively demonstrated. There are several disturbing discrepancies between observations and predictions based on the evaporation hypothesis. The quantitative arguments presented by the pro team are subject to large observational uncertainties and also depend on assumptions that at present cannot be verified. The blue-shifts that are observed may have an explanation in terms of the alternative model described above, although this is certainly not the only alternative explanation that could be proposed.

4.3.3 Recommendations for Further Research

The debate arguments given above have highlighted the strengths and weaknesses of present observations and theory. The purpose of this section is to summarize and recommend specific research that should clarify some of the problems concerning observation and theory that were discussed in the preceding sections.

Two specific experiments would shed considerable light on the role of evaporation in producing SXR flares. A weakness of the SMM experiment package is the low spatial resolution in SXRs. Similarly, weaknesses of the previous Skylab observations are the low time resolution and lack of hard X-ray spatial information. An experiment combining high spatial resolution ($< 3''$) in both hard and soft X-rays is clearly desirable. Also, it is desirable to have monochromatic soft X-ray flare images, as obtained by the NRL SO82-A slitless spectrograph on Skylab. However, because Doppler and spatial information are convolved in this instrument, a new experiment should consist of two such instruments, with the dispersions of their gratings at right angles to each other. Another way to achieve monochromatic spatial imaging in soft X-rays is to use the new technology of synthetic layer microstructures, i.e., multilayer coatings.

A second desirable experiment is to observe flares with X-ray crystal spectrometers that have considerably higher sensitivity than the present instruments on SMM, P78-1, and Hinotori. The reason is that when spectra are first observed with the present instrumentation, the electron temperature is already high ($> 10 \times 10^6$ K). Thus, the initial early times in the heating of the preflare loop or loops are not accessible to these instruments. Higher sensitivity can be achieved most easily by increasing the effective collecting areas of the crystals, whether bent or flat. Spectra obtained at onset of flare heating might enable the unknown preflare loop densities to be determined, from a study of line ratios sensitive to transient ionization and recombination. Also, the blue-shifted plasma is strongest at flare onset, and therefore the characteristics of the upflowing plasma can be studied with minimum contamination from stationary sources. A new crystal that might be used for some of these studies is InSb (Deslattes 1985). Crystals covering the resonance lines of Mg XI, Mg XII, Si XIII, Si XIV, S XV, S XVI, Ca XIX, Fe XXV, and Fe XXVI are desirable, in order to determine the properties of the blue-shifted plasma as a function of electron temperature.

On the theoretical side, there are several problems that need clarification. First, it would be highly desirable to numerically simulate a real flare, i.e., the flare rise time, loop length, electron temperature, density, and emission measure indicated by the observations should, by adjusting the energy input, and initial loop conditions, be imitated by the numerical simulation. In this way a direct comparison could be made between computed X-ray line profiles and observed profiles. Other theoretical problems involving fluid simulations that need investigation are the one-dimensional assumption of current numerical simulations, and the effects of magnetic field divergence on upflowing plasma. In terms of a particle model of flares, anomalous conductivity and the predicted ultrathin transition region need investigation. The thickness of the predicted transition region based on fluid models is less than the mean free path of the electrons, and the effects of this on both plasma dynamics as well as on spectral line intensities is presently unclear.

4.4 DEBATE OF ISSUE 2

The pro team adopts the hypothesis that a suitable chosen distribution of convective velocities associated with chromospheric evaporation can account for the major properties of both the blue asymmetry and the nonthermal broadening of X-ray lines during the impulsive phase of flares. If the hypothesis can be confirmed, the case that chromosheric evaporation has been directly observed becomes strong enough to proceed to a detailed study of the properties of evaporation and their relationships to theoretical models. If the hypothesis cannot be confirmed, the interpretation of both the blue asymmetry and the nonthermal broadening is called into question. Might the blue asymmetry be produced by motions that are non-evaporative, or are the tail of the evaporative distribution rather than its primary signature? Is the broadening seen during flares just an intensification of the process that causes ubiquitous broadening elsewhere on the Sun? If so, what does this imply about the commonality between flares and the "steady heating" of active and quiet regions? Magnetically driven gas motions are also a plausible candidate for the source of broadening in flares and in non-flaring regions. If magnetic motions are involved, the line broadening in flares is another piece of evidence that time-variable magnetic geometries play a fundamental role in the flare process.

Before beginning the debate both pro and con teams set forth the observed characteristics of the broadening that need to be explained. The following general properties of nonthermal broadening emerge from the sample of flares studied thus far with the current X-ray spectrometers (Antonucci *et al.*, 1982; Antonucci, Gabriel, and Dennis 1984, Doschek 1983):

a. The nonthermal broadening can be characterized approximately as isotropic Gaussian broadening with broadening parameters ξ (km s^{-1}).
b. $\xi_{max} = 150 - 300$ km s^{-1}, where ξ_{max} is the maximum nonthermal broadening measured during a given flare as observed in Ca XIX ($T_e \simeq 15 \times 10^6$ K) or Fe XXV ($T_e \simeq 30 \times 10^6$ K).
c. X-ray lines are broader than their thermal widths when first detected, before the peak of the hard X-rays.
d. The broadening diminishes markedly to $\xi \simeq 0 - 60$ km s^{-1} by the time of the SXR maximum. (The broadening may increase again later in the decay phase; the present discussion is limited to the impulsive phase.)
e. There appears to be no correlation between ξ_{max} and the position of the flare on the disk.
f. Broadening is also seen in lower temperature lines such as Fe XXI at 1354.1 Å ($T_e \simeq 10 \times 10^6$ K) and Mg XII at 8.42 Å ($T_e \simeq 7 \times 10^6$ K).

Other properties, less securely known or more difficult to quantify, or found for only a single event, were also identified during the debate. For example:

a. The maximum broadening appears to coincide with the peak of the HXR burst.
b. The lower temperature transition region lines such as C IV at 1550 Å also show non-thermal widths during the rise phase; however, the turbulent velocities deduced from the symmetric broadening of this line are markedly lower, less than 50 km s^{-1} than for the 10^7 K lines. Shine (Workshop contribution) has studied the UVSP observations of line profiles. Unfortunately there are few wavelength scans due to the nature of the instrument; however, the cases that he has been able to find all show a relatively low turbulent width in the $\simeq 10^5$ K lines. This is illustrated for three cases in Table 4.3. Note that higher velocities, greater than 100 km s^{-1}, are seen at times. However, these appear to be due to distinct and multiple emission features, probably from surge-like activity, and are not part of the symmetric broadening, which characteristically indicates a much lower velocity.
c. Leibacher has studied some SXR observations with high temporal and spatial resolution for two flares on November 5, 1980. Fortuitously, the lifetimes of the two flares overlapped such that the emission during the decay phase of the first event could be used as a wavelength reference for the emission during the rise phase of the second. The data show that at the earliest phase of the second event, its Ca XIX emission actually consists of a relatively narrow component, turbulent velocities $\simeq$ 80 km s^{-1}, but with a large blue-shift $\simeq$ 350 km s^{-1}. The blue-shifted line evolves by broadening and moving toward the red, so that after $\simeq$ 30 sec the emission from the second flare appears as a very broad line, turbulent velocity $\simeq$ 170 km s^{-1}, and centered at the rest wavelength.
d. Although there seems to be little variation in non-thermal widths from disk center to limb, Antonucci finds an average velocity of approximately 100 km s^{-1} for disk flares and 120 km s^{-1} for seven flares of longitude exceeding 70°. A larger sample of limb events is required to confirm this result.

Some of the above properties of line profiles are illustrated in Figure 4.9, based on BCS data analyzed by Antonucci *et al.* (1982). The quantity T_i is the temperature deduced from the linewidths, while T_e is the electron temperature deduced from line ratios. Nonthermal broadening is present when $T_i > T_e$. The figure shows the temporal behavior of the nonthermal broadening for the flare of 10 April 1980. The temporal relationship of this broadening to the hard X-ray burst is also shown. The debate on Issue 2 somewhat surprisingly turned out to be more difficult than the Issue 1 debate. The Issue 2 debate overlaps considerably with the Issue 1 debate because the origin of the X-ray blue-shifts was also discussed along with the nonthermal broadening. If the nonthermal broadening can be explained as due to a distribution of velocities of evaporating plasma, then the blue-shifts would presumably have an origin in the evaporating plasma as well.

4.4.1 Argument for: The Excess Line Broadening Is Due to Chromospheric Evaporation

The excess widths observed during the impulsive phase are almost certainly due to mass motions; however, the source of these motions is unknown. Arguments will be presented which strongly support the hypothesis that the observed widths are due to convective flows resulting from evaporation.

4.4.1.1 Amplitude of Evaporative Broadening Velocities

The numerical simulations to date have been concerned with the evaporation process in a single loop, rather than the distribution of velocities in a multi-loop arcade, as would be the case in any real flare. Hence, it is not yet possible to compare directly observed line widths, or profiles in general, with a particular simulation. However, the simulations of single-loop evaporation have some key results from the viewpoint of non-thermal line widths:

The velocities produced by the evaporation process are large. Some of the electron beam simulations find peak velocities along the magnetic field as high as 1000 km s^{-1}. Fisher has studied analytically the question of maximum evaporation velocities. He finds that from general arguments, the absolute maximum velocity that can be produced is approximately twice the sound speed of the evaporated material, which implies velocities of up to 2000 km s^{-1} for tem-

Table 4.3 Transition Region Line Widths for Impulsive Phase Flare Kernels

Line	Doppler Width	Event
O V 1371 A	37 - 46 km s^{-1}	Nov. 12, 1980 $\simeq$ 17:00 UT
O IV 1401 A	20 - 30 km s^{-1}	June 29, 1980 $\simeq$ 2:34 UT
Si IV 1402 A	20 - 30 km s^{-1}	June 29, 1980 $\simeq$ 2:34 UT

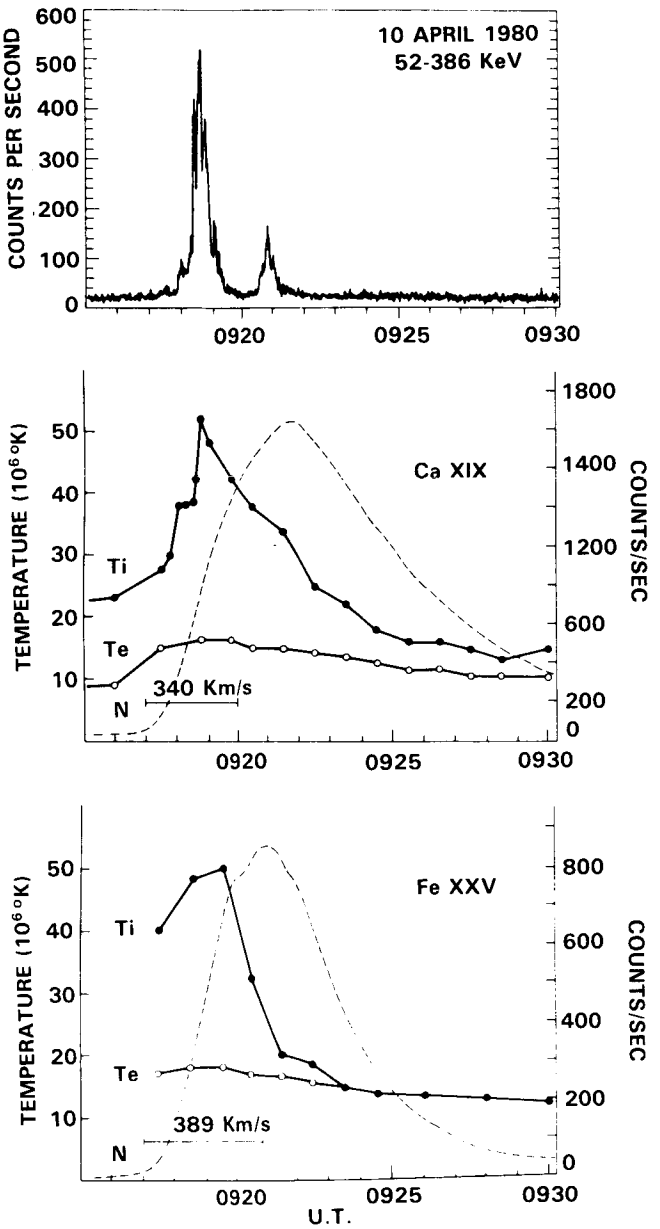

Figure 4.9 HXRBS and BCS results for the April 10, 1980 flare. T_i is a measure of the nonthermal broadening. See Antonucci *et al.* (1982) for details.

peratures of order 10^7 K. Of course, average velocities over the whole duration of the evaporation process will be significantly less than the above value; but, clearly bulk flow speeds of order several hundred km s^{-1} are to be expected from the evaporation process.

Another important result of the simulations is that, in general, the flows will not be all upward. If the flare heating and/or the loop geometry are not symmetric, as must be the usual case, then an evaporation flow from one foot point to the other will result. Cheng, Karpen, and Doschek (1984) have studied this process in detail by simulating a flare loop with an asymmetric heating function (see Issue 1 debate). As a result of this asymmetry the evaporation flow is stronger in the leg where the heat was deposited than in the other leg. The results of one of their simulations are shown in Figure 4.10 (see also Figure 4.5). The velocity profile along the loop is shown for various times. Note that initially upflows are present in both legs, but after approximately 30 s there are large downward flows in the unheated leg.

The final result pertains to the magnitude of the velocities at lower temperatures. Unfortunately, although the computed evaporation velocities at 10^7 K are fairly well known,

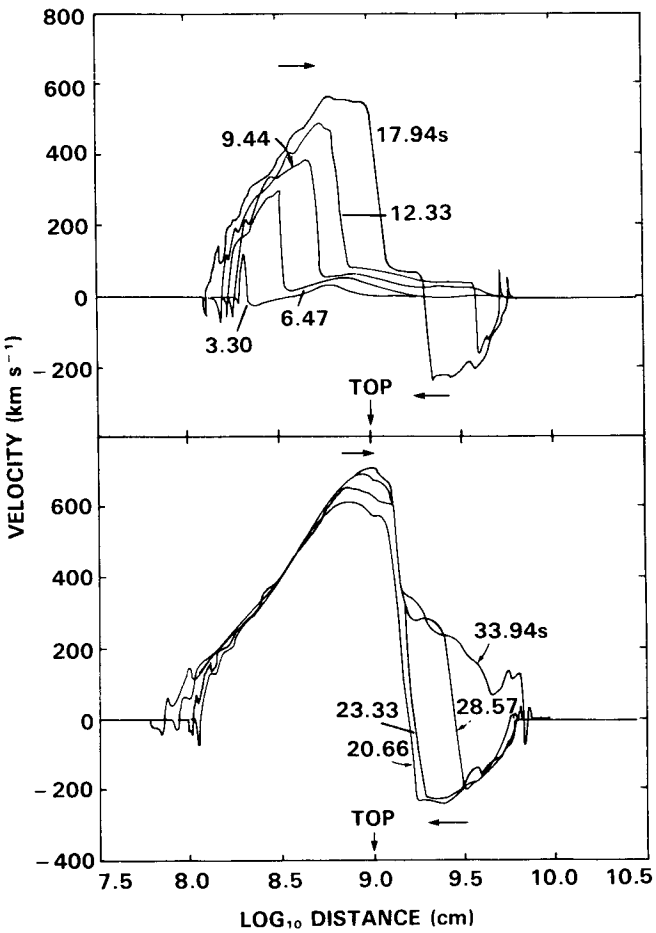

Figure 4.10 The fluid velocity as a function of position and time in the loop, from the numerical simulation of Cheng, Karpen, and Doschek (1984). Times are indicated in the figure. The top of the loop is also shown. Flare heating was deposited in a localized region about midway between the top of the loop and the left footpoint. Positive velocities indicate motion from left to right, i.e., upwards from the left footpoint. Negative velocities indicate upward motion from the right footpoint. The asymmetry between positive and negative velocities results from the asymmetric heat deposition.

those at 10^5 K are not. However, from quite general arguments evaporation velocities are expected to be of the order of the local plasma sound speed, so that the velocities at 10^5 K should be an order of magnitude or so less than those at 10^7 K. This result has been observed in the simulations that do resolve the transition region, albeit with lower impulsive heating than in a typical flare. Assuming that the flow speeds scale with the sound speed for larger heating rates as well, we expect evaporation velocities to be of order 50 km s^{-1} for material at 10^5 K.

4.4.1.2 Predicted Line Profiles

Qualitatively, the simulation results are in agreement with the observations. For a disk flare, both upflows and downflows should be observed, but with a stronger upward component since there is a net upward flow. Thus, 10^7 K spectral lines that are anomalously broad and with a blue excess are expected, and this is exactly what the observations show. The turbulent velocities should decrease with temperature, and again this is observed. At the limb we would expect to see instead of a blue excess a somewhat broader line, which also fits the observations.

Quantitatively, the agreement also appears to be good. First it must be emphasized that most solar flares do not consist of a single loop, i.e., a single activated flux tube. Flares generally have a complex magnetic geometry and a complex evolution. The observed emission at any particular time will be due to a distribution of loops, some of which may be in their evaporation phase, and others in their decay phase. Lacking accurate information as to the flare spatial and temporal structure, it is premature to attempt a detailed comparison of the evaporation model with the observed line profiles of any particular flare. Therefore the theoretical line profiles that have been calculated so far are only for idealized situations.

Leibacher has studied the effect on line broadening of the shear in velocity along a loop. He has taken one of the numerical simulations (Nagai 1980) and calculated the Ca XIX emission that would be observed by the XRP experiment from this loop model, including the instrument response. For the viewing angle he assumed the loop to be located halfway between disk center and limb, and inclined at an angle of 60 degrees to the solar vertical. Figure 4.11 shows the evolution of the Ca XIX line intensity and width as predicted by this model. Note that in agreement with observations, the width is largest when the rate of increase of the calcium emission is largest (see Figure 4.11f). Leibacher obtains the very interesting result that even a single loop can produce a spectrum that matches the observations.

Of course a single loop will produce a different line profile when viewed from different orientations. Since flares appear similar either at disk center or at the limb, a distribution of loops is required to fit all the observations. It is well known that all flares consist of a combination of loops.

Antiochos has studied analytically the line profiles expected from an arcade of loops. He investigated the idealized case of a distribution of loops of identical size and shape and with a constant velocity flow throughout each loop. The orientations of the loops, i.e., inclinations of the loops and directions of the lines joining the footpoints on the solar surface, are assumed to be completely random. Enough loops are assumed to be present such that there are no preponderances of loops at any particular inclination angle or in any particular direction. We call this distribution a hemispherically symmetric distribution. The loop plasma was assumed to be at a constant temperature and density. The flow speed was assumed to be four times the ion sound speed, or a flow speed of approximately 300 km s^{-1} for Ca at 10^7 K. The line profiles produced by such a distribution, when viewed at disk center and at the limb, are shown in Figure 4.12. In terms of velocities, the disk width is 120 km s^{-1} and the limb width is 280 km s^{-1}.

The important points of this work are that typical velocities of evaporated plasma can produce some of the observed widths, and that the widths should be larger at the limb. In fact the limb profile shown in Figure 4.12 is much wider than any limb profile that has yet been observed. Also it is distinctly non-Gaussian. This is due to the artificial distribution of loops and velocities that have been assumed. A hemi-spherically symmetric distribution favors horizontal loops, so that a large fraction lie parallel to the solar surface. Coupled with a constant flow speed throughout the loops, this assumption will produce very broad lines when such a distribution is viewed from the sides, i.e, at the limb. In reality we expect the distribution of loops to be peaked more toward the vertical than the horizontal, and the flow speed to vary both from loop to loop and within each loop. The plasma temperature and density will also vary in the same manner. These effects will make the velocities appear much more random, and hence, will lessen the difference between the widths at disk center and at the limb. Additionally, a more random distribution will produce a more Gaussian line profile.

Cheng has also studied the effect of a distribution of loops on line. He uses only a small number of loops, but with a much more realistic plasma model than used to generate Figure 4.12. The distribution of velocity, temperature and density along the loop are taken to be those at time = 28.57 s in his simulation of asymmetric flare heating (Figures 4.5, 4.10). Cheng has assumed three identical loops, all at disk center but inclined at angles of 0, 60, and 90 degrees to the solar vertical. The Fe XXV, Ca XIX, and Fe XXI line profiles produced by this combination are shown in Figure 4.13. Note than he finds not only a broadened line, but also a blue asymmetry due to the larger upward flow, as is observed. Again, the Ca XIX line profile in Figure 4.13 is wider than observed and is distinctly non-Gaussian. However, Cheng's assumptions are tantamount to having a flare in which all

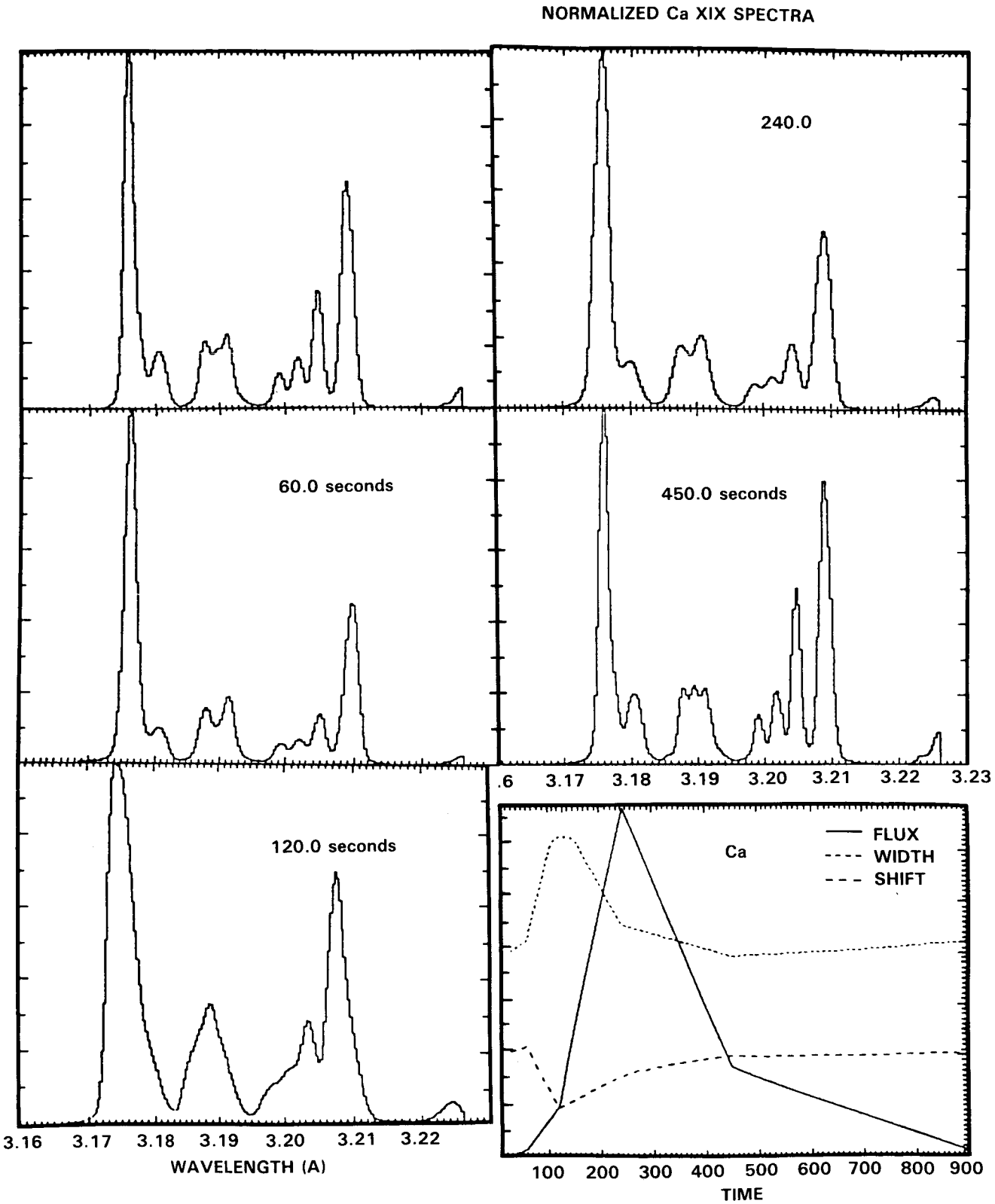

Figure 4.11 Profiles of the Ca line group computed from the simulation of Nagai (1980). See text for details.

the loops are heated simultaneously, and then observing these loops at their time of peak evaporation. More physical assumptions will yield profiles closer to observed ones.

It is reemphasized that the calculations presented above are for unrealistically simple models, so that they cannot be expected to predict line profiles that agree in detail with the observations. The key point of this work is that it demonstrates how easily evaporation can produce line broadening. Even the grossly simplified models above predict line profiles that begin to resemble the observed ones.

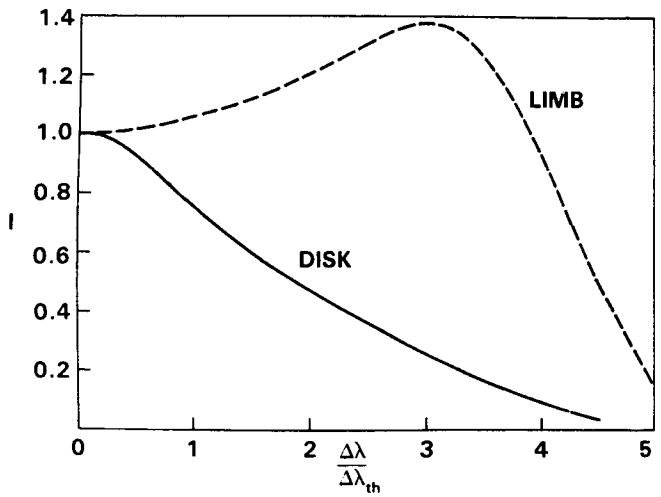

Figure 4.12 Computed Ca XIX resonance line profiles from the model by Antiochos (this Workshop). The profiles are computed for a disk flare and a limb flare. See text for discussion.

4.4.1.3 Discussion of evaporation versus MHD mechanisms

So far the only well-defined model for the anomalous line broadening is that it is due to convective motions in a distribution of loops. The main alternative to evaporation-driven convection is that the turbulent velocities are due to some form of MHD motions, perhaps related to prominence eruptions. However no definite model using MHD motions has been proposed; hence this alternative is presently little more than speculation. Keeping this vagueness of the MHD hypothesis in mind, it is nevertheless possible to compare the two competing models.

The observational and theoretical results presented above constitute a very strong case in favor of evaporation. The major points supporting this model are the following:

Evaporation provides a natural explanation for the observed tight correlation between line broadening and rise in soft X-ray emission measure. If evaporation is the cause of the turbulent velocities, then the line should be broadest when most of the emission is originating from evaporating material at the beginning of the soft X-ray burst, and the line broadening should disappear when evaporation ceases. This will occur within a few minutes after the maximum in X-ray emission measure, since the time scale for convective motions to decay is of the order of the travel time across the length of the loop, $\simeq$ 100 s for typical loop lengths and evaporative velocities.

There is no such clear explanation for the observations in terms of MHD motions. These are not well-correlated with the rise in X-ray emission measure. For large two-ribbon flares, such as the large flare on June 6, 1982 observed by Hinotori (Tanaka, Ohki, and Zirin 1985), the peak in MHD

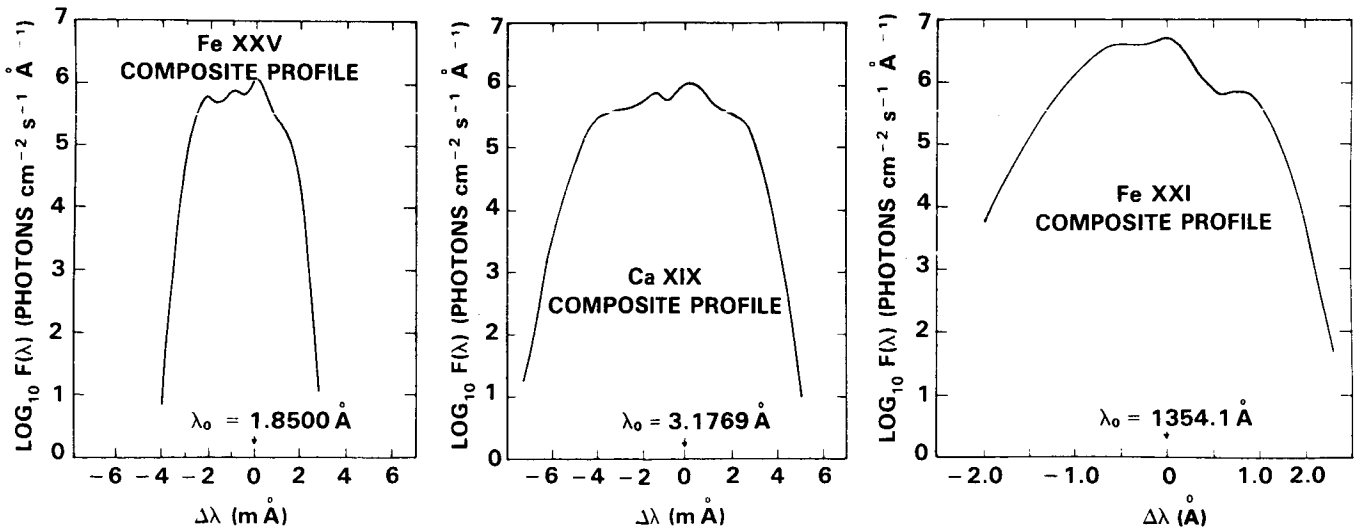

Figure 4.13 Line profiles predicted for an idealized 3-loop model based on the 1D simulations described in Cheng *et al.* (1983). The three loops are viewed at 0° (disk view), 60°, and 90° (limb view), respectively. The profiles are composites of all three loops. See text for discussion.

motions as indicated by the prominence ejection occurs well before the rapid rise in soft X-ray emission. Also, even if it is supposed that some form of MHD oscillations persists well after the prominence ejection, there is no good reason why such motions should end at the time of X-ray maximum. Alfven waves, for example should decay very slowly and would be present thoughout the flare duration. The magnitude of the turbulent velocities, and especially the strong temperature dependence of the velocities, are easily understood with the evaporative model. In evaporation the cool material always moves slower than the hot; hence, the line broadening will naturally decrease with decreasing temperature.

On the other hand, MHD flows often indicate the reverse situation, the most rapid velocities are in the coolest material. Sprays and prominence ejecta often show 10^4 K material accelerated to very high velocity, > 1000 km s^{-1}, far greater than any line shifts observed for the 10^7 K plasma. If MHD motions were the cause of the symmetric broadening, turbulent velocities at 10^5 K are expected to be as large or even larger than those at 10^7 K. To the knowledge of the pro team, this has never been observed.

Leibacher's observations of the November 5, 1980 flare provide further support for the evaporation model. The evolution of the Ca XIX line that he observed has no natural explanation in terms of MHD motions, but is exactly what is expected from evaporation. At the very earliest phase of a flare, the Ca XIX emission will originate from rapidly evaporating material in the first heated loop. For a flare at disk center a strongly blue-shifted line is expected, but without much broadening, just as is obtained from the single-loop simulations. Later in the event as the number of loops increases and the distribution of velocities becomes more complex, primarily a highly-broadened line should be observed.

From the theoretical work the major point supporting evaporation is that it can clearly produce broadening of the observed magnitude. The simulated line profiles all show at least as much width as is observed. If anything, the discrepancy is in the direction that evaporation is too efficient a broadening mechanism. MHD motions which are generally much faster than pressure driven ones would have an even greater difficulty in producing the relatively small (all quite subsonic) turbulent velocities inferred from the line widths. Note that any alternative model for the widths would first have to suppress somehow the strong evaporative broadening. Since evaporation is an almost inevitable consequence of flare heating, the pro team cannot see how evaporation can be suppressed.

In summary, the pro team concludes that evaporative motions are the cause of the anomalous line broadening. No doubt other models could be contrived that would also fit the observations, but these models would be just that — contrived. With the evaporation model, on the other hand, line broadening follows naturally from flare heating.

4.4.2 Argument Against: The Excess Line Broadening Is Due to Chromospheric Evaporation

The pro team of Issue 1 has argued that the blue-wing excess observed in X-ray lines during the impulsive phase is the signature of chromospheric evaporation. If this is correct, there is no question that "about the right" velocities (100-400 km s^{-1}) are present in the evaporating flow to broaden the main component of the line by "about the right" amount. As yet, the case for convective broadening has not advanced much beyond this statement of plausibility; and if the blue-wing excess is *not* produced by evaporation, the plausibility evaporates as well.

Antonucci has shown that there is a moderate correlation (product moment correlation $r = 0.7$) between the maximum blue-shift of the blue component in a given flare and the maximum nonthermal broadening in that flare (see Issue 1 debate). If nonthermal broadening is caused by evaporative flow, there should be correlations between the parameters of the blue excess and the parameters of the broadening. However, as usual, the presence of correlations is a necessary but not sufficient condition for the hypothesis; the parameters could be correlated through a common underlying phenomenon, not necessarily chromospheric evaporation.

The temporal correlation between the broadening and the blue component is not clear, largely because of observational difficulties. Spectra from P78-1/SOLFLEX (Doschek 1983) are created by scanning. Neither the total scan time ($\simeq$ 1 min) nor the time ($\simeq$ 10 s) required to scan through a line such as Ca XIX is negligible during the impulsive phase of a flare; this complicates the determination of broadening and the comparison of broadening and blue excess. With SMM/BCS data, it is often necessary to integrate over a comparable period of time (10-60 s) in order to build up enough signal to measure the blue component. Despite these difficulties, the observations do seem to indicate one aspect of the relationship between broadening and blue excess that is difficult to reconcile with the simplest picture in which the evaporative flow broadens the main component. Namely, the main component is sometimes measurably broadened for one or two minutes *before* there is any measurable blue component, and the degree of broadening may be as large ($\simeq$ 100 km s^{-1}) as at any time during the impulsive phase (Antonucci and Dennis 1983; Antonucci, Gabriel, and Dennis 1984). To maintain a causal relationship between evaporative flow and broadening, it would seem necessary to suppose that a blue component was present but for some reason not detected. This emphasizes the importance of thoroughly testing on noisy artificial data the algorithm used to fit the observed spectra (see Recommendations). We note that this result is the opposite of that found by Leibacher and discussed earlier. This difference may reflect a real difference among different flares, or perhaps it is partly due to the difficulty

of deconvolving moving and stationary components of a line profile at very early flare rise times, when the line intensities are very weak.

4.4.2.1 Single-loop Simulations

Before constructing a multiloop model, it should be shown that a single-loop simulation can provide a good description of the evaporative flow field; otherwise little confidence can be placed on the results produced by a superposition of such models. It should be kept in mind that the goal of a simulation is not just to produce a blue excess, or nonthermal broadening, but to reproduce their observed *relative* evolution. In the first approximation, the evolution may be characterized by $\xi(t)$, the nonthermal broadening parameter, by $v_{bl}(t)$, the speed of the blue-shifted component, and by R(t), the intensity ratio of the blue-shifted to the nearly unshifted ("main") component.

One good reason to stress relative behavior is that otherwise it is hard to know where in the time development of the model the observations begin. For example, in the centered-heating model of Cheng *et al.* (1983), for $t < 20$ s the blue-shifted component of Ca XIX dominates the unshifted component. Since this is never observed, one must either reject the model or assume that, because of the sensitivity limits of the detectors, the observations begin at a later stage.

The same model (Doschek *et al.*, 1983; Cheng *et al.*, 1983) can illustrate the danger of examining individual predictions in isolation. Figure 4.4 (see Section 4.3.2) shows the Ca XIX line profile 30.2 s after the onset of energy deposition. In a top view, the line shows a blue excess that would be fit by an evaporating component with $v_{bl} \simeq 200$ km s^{-1}, $R \simeq 0.2$. In an end view, the profile is convectively broadened by $\simeq 100$ km s^{-1}. These parameters are within the bounds of observation. However, at the same time ($t = 30.2$ s), the simulation predicts a gross shift of the Fe XXI line, about 150 km s^{-1} in the top view shown in Figure 4.4. As mentioned in Section 4.3, such shifts of the bulk of the emission have not been observed, either by Skylab (Doschek *et al.*, 1983) or by the UVSP aboard SMM (Mason *et al.*, 1985). We stress this disagreement to illustrate that the distribution of temperature and flow velocity in some single-loop models has points of serious disagreement with observation. It would therefore be premature to use such models as the basis for a multiloop simulation.

The comparison of Ca XIX and Fe XXI is an instance of a broader issue that needs more attention: the temperature dependence of the broadening, the blue excess, and the blue-shift of the main component. It does not appear that either existing observations or existing models have been probed sufficiently for the full extent of the information they might provide on this issue. The convective line broadening as a function of temperature can be considered in a general context, based on the simulations carried out to date. The following comments are probably independent of the simplifications of the 1D models, such as lack of transition region resolution and magnetic field tapering, etc. Assume for simplicity the case of a flare loop observed on the disk at zero longitude and heated symmetrically.

Consider first spectral lines formed over narrow temperature ranges with average temperatures of about $3 - 13 \times 10^6$ K. Ions such as Ca XVI, Ca XVII, Fe XXI, and Fe XXII are formed at temperatures within this range. After the loop or loops are filled with evaporated plasma these ions are formed near the footpoints of the loop and thus virtually the full spread in velocities will be observed. In the Cheng *et al.* (1983) simulation (Figure 4.4) $\xi \simeq 50$ km s^{-1} at 30.2 s. However, since the ions are formed over a relatively narrow temperature range, zero velocities (loop top) are not observed and all of the long wavelength XUV lines of these ions should show a net Doppler shift as well as a nonthermal broadening. Invoking a multiloop simulation will not remove the Doppler shifts, since in the evaporation model a *net* flow of plasma upward into the loops must occur.

Now consider the highest temperature lines observed, i.e., the resonance lines of Fe XXV and Fe XXVI. They are emitted primarily at the top of the loop in a symmetric simulation, where $\xi = 0$. Since the temperature of most flares is $\simeq 25 \times 10^6$ K, the line emissivities fall very rapidly towards the loop footpoints. Since the lines are formed near the loop tops, the Doppler shift and Doppler broadening tend to be much less than for the cooler lines, since motion is transverse to the line-of-sight. In the Cheng *et al.* (1983) simulation, $\xi = 35$ km s^{-1} for Fe XXV at 30.2 s.

Third, there is a group of lines such as the Ca XIX lines, that are formed at temperatures lower than Fe XXV, but higher than Fe XXI, and are formed over a broad temperature range. (Ca XIX is He-like). The Ca XIX lines are formed at the top of the loop as well as towards the footpoints. Thus these lines should show the maximum nonthermal broadening ($\simeq 86$ km s^{-1} at 30.2 s in the Cheng *et al.* (1983) simulation). They show a larger blue-wing than the hotter ions, but they have a strong stationary component.

Fourth, quiet and active coronal lines from ions such as Fe XIII - Fe XVI should produce broadening that might depend critically on the accuracy of the models near the transition region, since their temperature of formation ($\simeq 3 \times 10^6$ K) is near the turning point of evaporation and compression of the transition region. Similarly, transition region lines will be difficult to predict from the models for no other reason than that the transition regions have not been resolved in the numerical simulations.

In summary, symmetrically heated 1D loops produce non-thermal broadening that should be largest for lines such as Ca XIX and less for hotter (Fe XXV) and colder lines (Fe XVI). The innershell lines of Fe XXV, Fe XXIV - Fe XX should have different widths depending on ionization stage. On the contrary, the observations show large broaden-

ing for both Fe XXV and Ca XIX, with no significant decrease for the Fe XXV line.

Invoking an asymmetrically heated loop, rather than the symmetrical case, makes the situation even worse. Then downflows as well as upflows occur which broaden lines far beyond their observed widths (Cheng, Karpen, and Doschek 1984). Furthermore, the line profiles in a single loop model would exhibit central reversals for many lines. These could be eliminated in a multiloop model, but the lines would probably be widened even more. Basically, the numerical simulations of single loop models carried out so far indicate substantial discrepancies with the observations that appear to be independent of the physical and numerical simplifications at present necessary to carry out the calculations.

Another feature of loop simulations that should be examined is the blue-shift of the *main* component as a function of time. (As is stressed in the Recommendations section, the division into "blue" and "main" or "unshifted" components is an approximation.) By the time the main component earns its name (by dominating the blue component), its blue-shift is small (< 30 km s^{-1}); but Antonucci, Gabriel, and Dennis (1984) have reported tentative indications of shifts of this order in the main component. If such shifts are confirmed, they bear on the broader question (Issue 1) of whether the observed blue excess is the primary signature of chromospheric evaporation. Antonucci *et al.* (1982) and Antonucci and Dennis (1983) have shown that reasonable densities ($n_e \simeq 5 - 10 \times 10^{10}$ cm^{-3}) are inferred for the blue component if it is assumed to supply the mass necessary to produce the observed emission measure. However, densities an order of magnitude higher are not ruled out, and if the same argument is applied in reverse, small evaporative velocities ($v_{bl} \simeq 10 - 40$ km s^{-1}) are inferred. The primary signature of evaporation would then be the small shift in the fitted wavelength of the main profile; what is here termed the blue component would be a high velocity tail or a secondary phenomenon, not the primary signature.

4.4.2.2 Multiloop Models

Two key observational points are that the broadening in each flare is approximately isotropic, and that the degree of broadening shows no strong trend with the position of the flare on the disk. Since, as might be expected, the line profiles produced by single-loop simulations of chromospheric evaporation show a marked dependence on the vantage point (Figure 4.5), a multiloop model is required to even approach a resemblance to the observations. Unfortunately for the pro side of this debate, a necessary characteristic of a multiloop model that is needed to satisfy the observations is generally a random orientation of the loops. Only in this way can the observational requirement of isotropy in the line widths be satisfied. However, although most flares are known to consist of several loops, the orientations of the loops are *not* usually random. Typically arcades of loops are involved, all oriented in the same sense. In this case it is expected that the line broadening would vary considerably among different flares, particularly between disk and limb flares. However, this is not observed. Furthermore, in order to explain the strong stationary components of lines such as Fe XXI, at least one loop is required that lies almost flat on the solar surface so that Doppler shifts are negligible. This can hardly be satisfied by all flares. And finally, the resultant line profiles (Figure 4.13), although greatly broadened, do not resemble Gaussian profiles, contrary to the observations.

Unlike the nonthermal broadening, the blue excess is correlated with position on the disk: no flare located more than 60° from disk center has shown a detectable blue excess (Antonucci and Dennis 1983). In terms of a multiloop model, this implies that the blue excess is produced by X-ray hot gas that is still close to the footpoints of loops that emerge roughly perpendicular to the surface, while the broadening of the main component is produced by gas higher up in the loop. This is logical, but no multiloop models exist to demonstrate quantitative agreement with the observations.

4.4.2.3 Broadening Caused by Mechanisms Other than Evaporation

Nonthermal broadening of UV and X-ray lines is not confined to the impulsive phase of flares. On the contrary, nonthermal broadening is ubiquitous in non-flare spectra; only in quiescent prominences is there no evidence for $\xi > 0$ (Feldman and Doschek 1977). In quiet regions and coronal holes, $\xi \simeq 20 - 25$ km s^{-1} in the lower transition region (Doschek, Mariska, and Feldman 1981) and $10 - 25$ km s^{-1} in the corona (Cheng, Doschek, and Feldman 1979). In active regions, $\xi \simeq 30 - 50$ km s^{-1} in the lower transition region (Brueckner 1975) and $\xi \simeq 75$ km s^{-1} for preflare brightenings in Ca XIX (Antonucci *et al.*, 1982). These broadenings appear to be isotropic: no differences have been established from center to limb.

Since isotropic broadening is observed nearly everywhere on the Sun, in both quiet and active regions, is it not perverse to invoke chromospheric evaporation — a mechanism usually involved only during flares — for flare-associated broadening? Would it not be more unifying to suggest instead that whatever processes cause the ubiquitous broadening are simply enhanced in flares, as are so many other processes? The cause of the ubiquitous broadening is unknown ("turbulent broadening" is at best a label, and perhaps a misnomer), but there is no reason to suppose that it is connected with chromospheric evaporation. Whatever the broadening mechanism, if it is the same in flares and nonflaring regions, it suggests a basic similarity between flares and "steady" atmospheric heating.

Magnetically driven motions should be considered as a specific alternative to evaporative motions as the source of nonthermal broadening. In cine Hα observations of flares, it is commonplace to observe motions with $v \simeq$ 100-200

km s^{-1} that appear to be motions of the magnetic field lines (together with their frozen-in plasma) rather than the flow of gas along stationary field lines. Moreover, these magnetic motions often appear to have an "unwinding" component, particularly evident in filament eruptions. Figure 4.14, a time-sequence of Hα observations, illustrates the complicated motions that accompany overall expansion during a flare. The broadening produced by such motions would have "about the right" value (a property shared by the evaporative hypothesis) and would also be approximately isotropic, as is observed. Unlike a postulated distribution of evaporative velocities, however, magnetic motions are observed, not only during flares but, to a lesser degree, all over the Sun. As to the relative timing of flare-associated broadening, it is relevant to cite the results of Martin and Ramsey (1972), Moore *et al.* (1984) and Moore and Kahler (1984), that the fastest motions during a filament eruption usually occur at the peak of the impulsive phase.

There is one example that supports the importance of magnetic motions in the production of line broadening. Using data from the NRL slitless spectrograph aboard Skylab, Widing (1975) claimed that in the double ribbon flare of June 15, 1973, the area of greatest broadening in Fe XIV and Fe XXIV occurred over the magnetic neutral line, coincident

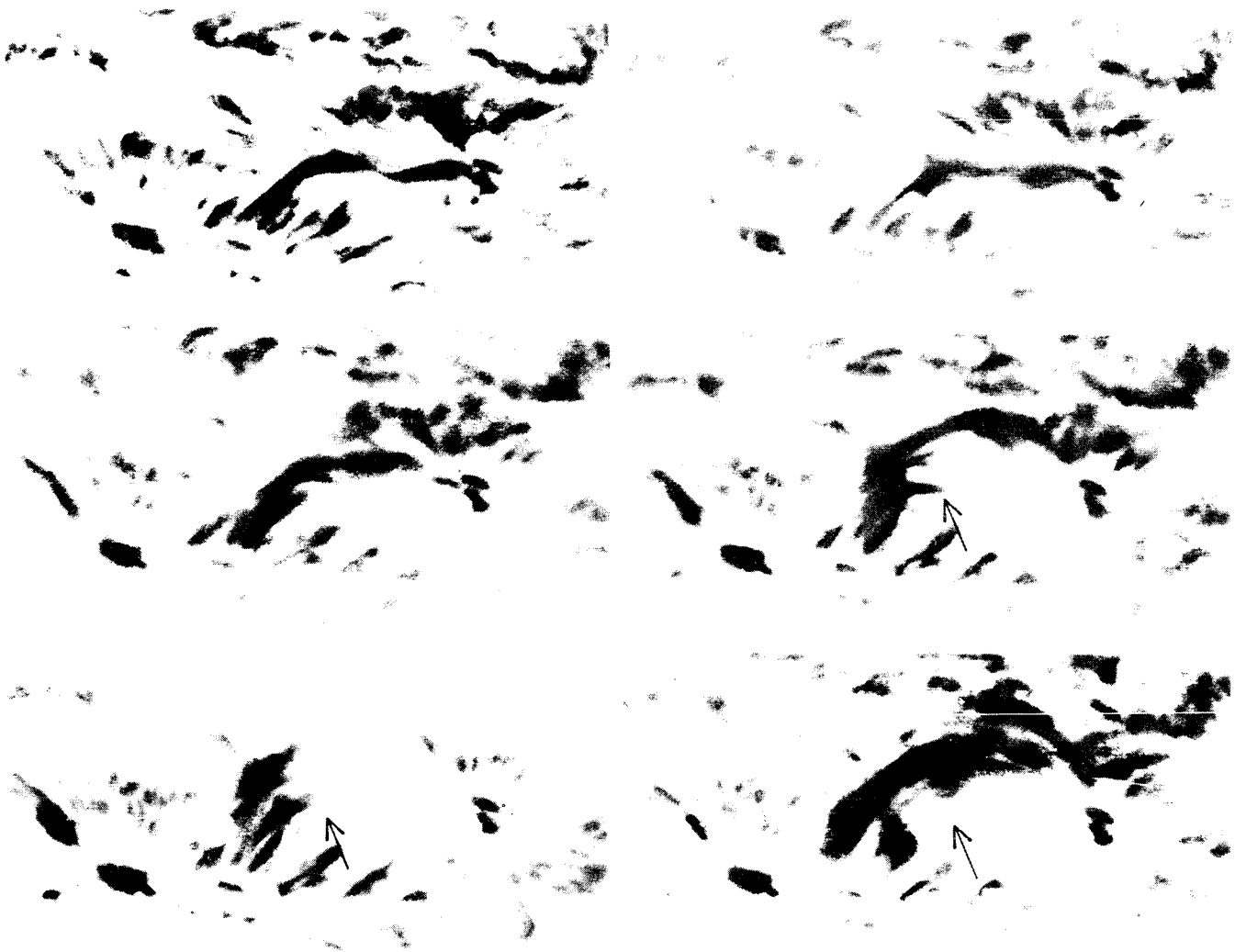

Figure 4.14 Complex motions of the magnetic field in a flare of 27 April 1972. Filtergrams 0.8 Å in the blue wing of Hα from the Big Bear Solar Observatory. The long dimension of the frames corresponds to approximately 10^5 km. The time sequence shows an overall expansion of the loop system at a peak velocity of about 70 km s^{-1}. The arrow in the frame at 1638 UT points to a dark feature that curves off to the left. The arrows in the frames at 1639 UT and 1643 UT are placed at the same spatial location as the first arrow. The dark feature shows motions of 75-100 km s^{-1} that have components in three directions and cannot be characterized as simple expansion. Note that at 1639 UT the dark feature appears to be braided with another dark feature, but by 1643 UT no braiding is apparent.

with a filament eruption -- not at the footpoints of a loop. This possibility needs to be confirmed with future imaging instruments (see Recommendations).

Except in flare sprays, magnetic motions during flares with $v > 300$ km s^{-1} are uncommon, or at least uncommonly observed in Hα. Thus, it is not clear that magnetic levitation of heated material can account for the blue component of X-ray lines, for which $v_{bl} > 300$ km s^{-1} is typical. If the blue component is in fact due to evaporation, the magnetic motion alternative for broadening precludes the simplest kinematic picture in which both broadening and blue excess are produced by a common velocity field.

In summary, the hypothesis that convective evaporation produces the observed X-ray line widths in flares is no more than a hypothesis. It is not supported by any self-consistent physical theory. In fact, the 1D numerical simulations, although they indeed produce excess line broadening, predict relative widths and shifts that are not in agreement with the evaporation hypothesis. These disagreements are independent of the simplifications in the calculations.

4.4.3 Recommendations for Further Research

All but one of these recommendations can be pursued now, by theoretical work or with data from the repaired SMM, P78-1, or Hinotori. The last recommendation concerns the capabilities of a future spaceborne instrument designed to advance our understanding of the physics of the broadening and blue excess of X-ray lines.

a. Clarify the relative time evolution of the broadening and the blue excess of X-ray lines (both observations and models).
b. Clarify the temperature dependence of the broadening and the blue excess (observations and models).
c. Publish a detailed analysis of the performance of algorithms used to fit the observed spectra, including:
   i. Minimum detectable v_{bl} and accuracy of determination of ξ as a function of S/N (signal-to-noise ratio), v_{bl} and R.
   ii. Minimum detectable v_{bl} and accuracy of determination of v_{bl} as a function of S/N, ξ, and R.
   iii. Minimum detectable R as a function of S/N, v_{bl} and ξ.
   iv. Correlations between fitted values of ξ, v_{bl} and R.
   v. Minimum detectable velocity shift in the main component.
   vi. Sensitivity of fitted parameters to the assumed electron temperature and broadening of the blue component (since the data are not sufficient to determine these parameters independently). It should be remembered that two-component fitting is always an approximation to what is undoubtedly a continuous distribution of velocities. When better loop simulations become available, it will be worth experimenting with velocity-amplitude distribution functions.
d. Using the results of Recommendation c, determine whether small blue-shifts (< 40 km s^{-1}) have been detected in the main component.
e. Determine for each instrument the absolute flux threshold at which a blue excess can be detected. It is important to understand why only one or two flares have been observed in which the blue-shifted component is nearly as strong as, or stronger than, the "stationary" component.
f. Examine Hα movies of flares also observed by X-ray spectrometers for evidence of magnetically driven motions.
g. Obtain spatially resolved SXR spectra. The relative locations of the plasma producing the blue excess, the broadened main component, and the HXRs will go a long way toward deciding the influence of chromospheric evaporation on the X-ray line profiles. Suggested characteristics of the detector are:
   i. Angular resolution $< 2''$.
   ii. Temporal resolution < 10 s.
   iii. Spectral resolution < 0.3 mÅ, comparable to that of existing spectrometers.
   iv. Spectral ranges similar to those existing and previous instruments; it is important to include lines with characteristic temperatures in the range $1 - 10 \times 10^6$ K, as well as higher temperature lines.

4.5. DEBATE OF ISSUE 3

At the present time, there are basically two models concerned with how the energy could be transported to the chromosphere in order to drive the chromospheric evaporation process. One of these models, the nonthermal electron thick target model (Brown 1973), proposes that energy during the impulsive phase is supplied by a large flux of energetic electrons, whose source is generally supposed to be in the corona. It is also generally supposed that the electrons are accelerated to their high energies by rapid reconnection of coronal magnetic fields. In this model, the chromosphere is heated by Coulomb collisions from the flux of nonthermal electrons, and the chromospheric radiative output increases and evaporation can occur. Another model, the thermal conduction model, supposes that only the corona is heated during the impulsive phase, and that energy deposited in the corona drives evaporation from the chromosphere by thermal conduction. In the conduction model, the energy release can occur at various positions within coronal flux tubes, and could also be due to a reconnection process. The chromosphere is heated when a conduction front, generated at the site of energy release, propagates downward along the flux tube and deposits energy into the chromosphere. As with the beam model, the chromosphere reponds to this heat input both radiatively and dynamically.

Because thermal conduction and high energy electrons represent two different modes of energy transport and energy deposition into the chromosphere, the responses of the chromosphere to each of these modes of energy deposition should be different, at least to some degree. In the debate given below, one of the central issues is whether or not the physics of beam and conduction energy deposition is well enough understood such that the available observations can be used to decide which mode of energy deposition is more important in producing chromospheric heating during flares. Another central issue is, assuming that beam and conduction energy deposition physics is known very well, whether or not the observations are of sufficient quality to resolve differences between beam and conduction heating, and if not, what further observations are needed.

4.5.1 Argument for: Most Chromospheric Heating Is Driven by Electron Beams

In this position paper, the evidence in support of evaporation by the nonthermal electron thick target mode is examined. In Section 4.1, evidence is discussed which argues in favor of the thick target model from a comparison of spatial and temporal relationships between HXR emission, SXR bremsstrahlung, SXR line emission, EUV radiation from transition region temperatures, and Hα line profiles emitted from the chromosphere. In the subsequent two sections, some possible observational characteristics predicted by theoretical calculations of chromospheric evaporation by the thick target model are discussed. Section 4.2 begins with a review of what has been learned from numerical simulations of chromospheric evaporation. In Section 4.3, some possible evidence for hydrodynamic features predicted by the electron beam simulations is presented. Finally, the position of the electron beam team is summarized in Section 4.4.

4.5.1.1 Evidence of Impulsive Phase Emission from Observed Temporal and Spatial Relationships

a. Hard and soft X-ray bremsstrahlung. One of the reasons frequently invoked in favor of flare heating by nonthermal electrons is the relative timing of HXR and SXR emission. The peak in HXR emission during flares generally preceeds the peak in SXR emission. Qualitatively, this process is envisioned as follows. As bursts of nonthermal electrons generated by impulsive phenomena in the corona impinge on the chromosphere, nonthermal bremsstrahlung from the fast electrons is produced, giving rise to observed HXR bursts. As the fast electrons deposit their energy in the upper chromosphere, the chromospheric material is heated to coronal temperatures and subsequently expands to fill a coronal loop structure. As the loop fills with hot evaporated material, emission by thermal bremsstrahlung in the SXR spectral range increases (Nagai 1980). When the bursts of nonthermal electrons cease, the evaporation process allegedly stops, and the SXR emission measure reaches its peak value. As the coronal material cools by radiation and thermal conduction, the SXR emission begins to drop. Some aspects of these speculations are verified by detailed studies and others are not.

Although the HXR and SXR timing aspects of this picture hold true for a large number of flares, there are certainly examples of flares for which HXR and SXR emission do not appear to be causally related in the above manner (Svestka 1976).

For several particularly well observed flares, however, it is possible to go beyond the qualitative picture and compute the energy content of nonthermal electrons from HXR intensities and footpoint sizes observed by HXIS. This can then be compared to the thermal energy content in the heated coronal material, deducted by SXR spectra from Ca XIX lines and thermal bremsstrahlung. Antonucci, Gabriel, and Dennis (1984) (hereafter AGD) have done this for five large events observed by SMM. After correcting for radiation and conduction losses, they find that the energy content in nonthermal electrons is quite compatible with the thermal energy observed in these flares. These results are shown in Table 4.2.

b. Hard X-rays and soft X-ray line emission. The most obvious interpretation of the blue-shifted components of X-ray lines is the upward expansion of "evaporated" material into the flare corona. Antonucci and Dennis (1983) compellingly argue for this interpretation by correlating the upward velocity inferred from Ca XIX blue-shifts for a number of different flares with the rate of change of SXR emission measure in each flare. AGD have also presented evidence that these blue-shifts are casually related to the presence of energetic electrons. The onset of the blue-wing asymmetry in Ca XIX line profiles coincides with the onset of HXR emission for the flare analyzed by these authors. This behavior is illustrated by Figure 4.1 (Section 4.3.1), which shows the temporal evolution of HXR emission, the velocity of the blue-shifted component, and the SXR emission measure for the May 21, 1980 event (AGD 1984). The fact that the blue-shifted material appears at the onset of HXR emission and disappears when HXR emission ceases argues strongly that upward coronal velocities associated with impulsive phase chromospheric evaporation are somehow powered by energetic electrons.

c. O V emission and hard X-rays. Evidence supporting the validity of the thick target description of chromospheric evaporation is the observation by SMM of a tight correlation in time between individual bursts of O V EUV emission and HXRs (Woodgate *et al.*, 1983). The delay in individual O V bursts relative to HXR bursts in some flares is observed to be less than one second. These time delays are short enough to argue that the same energetic electrons responsible for HXR emission must also be responsible for the O V emission. This time correlation is difficult to explain if chromospheric evaporation is driven entirely by thermal conduction. Time delays of at least several seconds are

typically seen in numerical simulations of conductive driven evaporation, where flare energy release is confined to the corona. This appears to be true even when the loop lengths are fairly short (Nagai 1980, Cheng *et al.*, 1983, Pallavicini *et al.*, 1983). We note that O V observations should be made carefully, since the O V line contains some spectral blends. These blends are discussed by Jordan (1985). (Also, see the flare line list published by Cohen, Feldman, and Doschek 1978).

d. Hα emission and hard X-rays. Evidence that nonthermal electrons are involved in the chromospheric evaporation process comes from observations of chromospheric (Hα) line profiles during the impulsive phase of flares. The nonthermal electron thick target model predicts that the residual (unevaporated) flare chromosphere should be heated significantly by the imposed flux of nonthermal electrons (Brown 1973, Ricchiazzi and Canfield 1983). If, on the other hand, the only chromospheric heating mechanism invoked during the impulsive phase of flares is thermal conduction from the corona, it can be shown (Ricchiazzi and Canfield 1983) that the temperature structure of the unevaporated portion of the chromosphere is virtually unaffected. Since Hα profiles are formed in the flare chromosphere, observations of Hα profiles during flares yield useful information about the nature of the impulsive phase heating mechanism.

Calculations of Hα profiles by Canfield, Gunkler, and Ricchiazzi (1984) show distinct features of these profiles which can be linked to conditions in the flare chromosphere. One important result is that only the presence of nonthermal electrons can produce broad Stark wings, typically 1 to 5 Å away from line center. Recent observations of Hα profiles during flares were made at Sacramento Peak Observatory in conjunction with SMM observations (Acton *et al.*, 1982, Gunkler *et al.*, 1984, Canfield and Gunkler 1984). These observations show strong Stark-like wings in the Hα profiles coinciding spatially and temporally with hard X-ray emission observed by the HXIS instrument onboard SMM. These observations strongly suggest that nonthermal electrons heat the residual chromosphere during the impulsive phase of flares.

4.5.1.2 Some Results of Hydrodynamic Calculations

A number of theoretical hydrodynamic calculations of chromospheric evaporation in flares have been done, both for flare heating by nonthermal electrons, and for "thermal conduction" models where all or most of the energy is deposited in the corona. Since these calculations may shed some light on various aspects of the observations, the results of these calculations are now reviewed.

a. Thick target electron-driven evaporation. Numerical studies of chromospheric evaporation due to heating by collisions from an assumed flux of nonthermal electrons have been done by a number of authors (Kostyuk 1976, Kostyuk and Pikel'ner 1975, Somov, Syrovatskii, and Spektor 1981, Livshitz *et al.*, 1981, Duijveman, Somov, and Spektor 1983, Nagai and Emslie 1983, MacNeice *et al.*, 1984, Fisher, Canfield, and McClymont 1985a). These results show that evaporation driven by beams can be divided into two regimes, depending on the magnitude of the thick target energy input flux. Below a certain critical energy input flux, flare heating balances radiative losses everywhere in the flare chromosphere. The temperature in the flare chromosphere is raised a moderate amount by the thick target heating, but does not exceed 10^5 K. Hydrodynamically, the chromosphere responds to this moderate temperature increase by expanding upward. In the meantime, the flare heating in the corona raises the temperature there, increasing the conductive flux into the transition region. This slowly drives the transition region into the chromospheric material on coronal conductive timescales. This evaporation scenario is called "gentle" evaporation, because of the relatively gentle response of the atmosphere to the imposed heating function.

The threshold above which gentle evaporation no longer occurs can be found by setting the flare heating rate (per particle) at the column depth of the chromospheric material just below the preflare transition region equal to the product of the density there with the peak in the radiative loss function near $T = 10^5$ K. This procedure, suggested by Brown (1973) and Lin and Hudson (1976) has been verified with numerical calculations by MacNeice *et al.*, (1984) and Fisher, Canfield, and McClymont (1984c), though an important modification has been suggested by McClymont, Canfield, and Fisher (1985), taking into account closed loop geometry and preflare coronal pressure.

When the flare energy input rate exceeds this threshold, the chromospheric material just below the preflare transition region is no longer able to radiate away the energy being supplied to it by the flare heating function. The material then rapidly heats up to coronal temperatures *en masse*. Since the time scale for this rapid temperature rise is usually short compared to hydrodynamic timescales in the heated region, this creates a large overpressure coinciding with the rapidly heating region. The heated material then expands explosively into the coronal material above it, at speeds near (roughly 60% to 100%) the $2.35c_s$ upper limit identified by Fisher, Canfield, and McClymont (1984). The quantity c_s here is just the sound speed in the explosively evaporated material. For this reason, we describe this scenario as "explosive" evaporation. Not only does the large overpressure drive the heated material upward, but it also drives mass motion downward into the flare chromosphere. Thus, velocities in the upper flare chromosphere are downward for explosive evaporation, in contrast to the upward velocities expected during gentle evaporation. This difference in sign of hydrodynamic velocities between explosive and gentle evaporation holds as well for velocities computed in the lower transition region, at temperatures around 10^5 K. In addition, it has been shown by Fisher, Canfield, and McClymont

(1985a) that the downward moving region of the flare chromosphere during explosive evaporation must be cold and dense relative to its surroundings. This feature has been seen, though not properly explained, in a number of numerical simulations. Furthermore, this downward moving "chromospheric condensation" accretes matter very quickly, encompassing in a few seconds more material than is moving upward.

b. Conduction-driven evaporation. It has long been recognized that thermal conduction should be a very important mechanism for the evaporation of chromospheric material during flares. If we assume that thermal conduction is the only mechanism responsible for chromospheric evaporation, and that there is no other heating mechanism for the flare chromosphere other than quiescent heating, then it is possible to show that there are some differences between this and evaporation driven by nonthermal electron heating.

A number of numerical simulations have been done of chromospheric evaporation by thermal conduction (Nagai 1980, Somov, Sermulina, and Spektor 1982, Cheng *et al.*, 1983, Pallavicini *et al.*, 1983). These calculations typically show evaporation driven velocities of about half the sound speed, or at about 20% of the $2.35c_s$ upper limit. In recent simulations such as the revised SMM benchmark calculations, it can be seen that there is a very thin chromospheric condensation which stays just ahead of the moving conduction front. The conduction front plows its way through the chromosphere at a nearly constant mass flux rate. Just in front of the thin condensation, the hydrodynamic velocities, temperatures, and densities are unchanged from those before the flare. In the thin condensation itself, hydrodynamic velocities are downward, just as they were in the case of the chromospheric condensation formed in explosive evaporation by nonthermal electrons. One important difference, however, is that the thickness of the condensation for conduction driven evaporation is small at all times, at least in the revised SMM Benchmark calculation. The moving conduction front eats up the back end of the condensation nearly as quickly as the front of the condensation moves through the chromosphere. The velocities in the conduction front at transition region temperatures are downward. The temperature at which the velocity changes sign in this calculation is around 2×10^6 K. Importantly, there seems to be no threshold heating rate for which hydrodynamic velocities in the chromosphere or the transition region would change sign, as there is for evaporation by nonthermal electrons. Therefore, examination of velocities at transition region and chromospheric temperatures should yield important information about the nature of flare heating.

4.5.1.3 More Evidence in Favor of Evaporation by Nonthermal Electrons

From the theoretical hydrodynamic calculations, it is clear that one possible way to differentiate among flare heating mechanisms is to look for observational evidence of "explosive" evaporation. Such evidence could include the existence of upflow velocities near the $2.35c_s$ limit, or the sudden appearance of high densities at high coronal temperatures and their subsequent relaxation to lower values on coronal loop hydrodynamic time scales. Another possibility is to look for evidence of the threshold between "gentle" and "explosive" evaporation by looking for spatial changes of sign in observed velocities at chromospheric temperatures and comparing these with what is expected from observed fluxes of energy in nonthermal electrons. These effects should not be seen for conductive driven evaporation. Possible observations of explosive evaporation are not outlined.

a. Density near 2×10^6 K as a function of time. Doschek *et al.* (1981) derived the electron density near $T = 2 \times 10^6$ K as a function of time for the 8 April and 9 May 1980 flares, by analyzing emission from a forbidden transition of O VII seen from the P78-1 spacecraft during these flares. They find that the electron density increases by at least a factor of ten in a time no longer than a minute. The peak values of density, about 10^{12} cm^{-3}, are consistent with preflare chromospheric values. The electron densities then gradually decay in value over a timescale of several minutes.

Qualitatively, this is the scenario expected from explosive evaporation by nonthermal electrons, although the timescales are somewhat longer than predicted. As a portion of the chromosphere is rapidly heated *en masse* from chromospheric to coronal temperatures, the material is expected to pass through temperatures near 10^6 K while still at chromospheric densities. As the explosively heated material begins to expand, however, the density of this region should decrease. If evaporation is postulated as being due to a conduction front which impacts the chromosphere and then moves downward through it in a self similar fashion, the density near 10^6 K might be expected to suddenly increase, but to then maintain a more or less steady value as long as evaporation continues. Furthermore, unless the conduction front is moving exceedingly quickly, some hydrodynamic expansion would be expected to occur by the time that the material was heated up to 2×10^6 K, so that the densities would be noticeably less than chromospheric values.

b. Impulsive phase asymmetries in Hα profiles. Ichimoto and Kurokawa (1984) have recently reported that they see significant enhancements of red-wing asymmetry in Hα profiles observed during the impulsive phase of flares. They find that this red wing asymmetry corresponds to downward motion at Hα emitting regions of the chromosphere, with velocities between 40 and 100 km s^{-1}. These downward velocities are similar in magnitude to those seen in numerical flare simulations of explosive evaporation by nonthermal electrons. They claim downward motion in conduction model calculations, e.g., Cheng *et al.* (1983), does not produce sufficiently strong downward velocities to match

those they measure from the asymmetries. Ichimoto and Kurakawa (1984) therefore conclude that they are seeing downward moving chromospheric condensations associated with explosive evaporation by nonthermal electrons.

4.5.1.4 Conclusions

The evidence in favor of driving chromospheric evaporation by fluxes of nonthermal electrons has been reviewed. It is found that there is enough energy in energetic electrons to power the SXR portion of the flares during the impulsive phase for five well observed flares. The observed blue-shifts in Ca XIX line profiles, which can be interpreted as signatures of chromospheric evaporation, begin with the onset of HXRs and terminate cotemporally with the HXR flux. Individual spikes of O V emission formed at transition region temperatures track corresponding spikes in HXR emission to better than one second. Hα profiles with Stark-like wings, indicating the presence of energetic electrons, are found to be cospatial and cotemporal with the HXIS images of HXR emission. Taken together, these finds strongly suggest that energetic fluxes of electrons penetrate deep into the solar atmosphere and are intimately connected to the chromospheric evaporation process.

4.5.2 Argument Against: Most Chromospheric Heating Is Driven by Electron Beams

The case for direct electron beam heating and subsequent evaporation of the chromosphere originally rested on the thick-target interpretation (Brown 1973) of HXR bursts and on the finding by Lin and Hudson (1976) that the electron beam energy, as calculated with the thick-target model, was greater than the coronal flare plasma energy in a number of large flares. Two important recent findings apparently have bolstered the case for direct electron beam effects in the chromosphere, namely, the close correlations found between hard X-ray and UV emissions (Woodgate *et al.*, 1983), and the interpretation of Stark-Broadened Hα line profiles in terms of electron heating (Canfield, Gunkler, and Ricchiazzi 1984, Canfield and Gunkler 1985, and Gunkler *et al.*, 1984). However, the thick-target model and arguments for chromospheric heating based only on energetics encounter severe difficulties when examined in detail. Furthermore, the recent UV and Hα results, while they argue for the existence of electron beams, do not prove that electron beams drive most chromospheric evaporation. A detailed discussion of these points is presented in the paragraphs that follow, starting with questions about the reality of the beams themselves. Then follows a discussion of UV and SXR observations that do not support the beam evaporation model. They tend, instead, to support a coronal heating/conduction-driven explanation of evaporation. Finally, computer simulations of flares are considered. The results are compared with observations of blue-shifts in SXR lines and of Hα line profiles. The results support conduction as the principal driver of evaporation, even when there is some evaporation of the upper chromosphere by a flux of nonthermal electrons.

4.5.2.1 Evidence Against Electron Beams

The reexaminations of the thick target model presented elsewhere in this book indicate that electron beams with the energy and dimensions required by observations may not be stable. The instabilities considered most likely to occur in intense beams will cause them to dissipate their energy as heat in the corona in a very small fraction of a second. But, as of now, there is no direct evidence that intense electron beams even exist in the corona. Attempts to measure polarization of X-rays have given either negative results, or the published positive results are suspect. Similarly, attempts to infer anisotropic X-ray emission indirectly by center-to-limb observations of flares have given negative results (e.g., Kane *et al.*, 1982), although this result does not rule out some beam models. It simply means that highly anisotropic HXR emission is not observed. Thus, belief in electron beams must ultimately rely on belief in theoretical arguments.

If beams exist and if they reach the chromosphere, it is clear that they are short-lived phenomena and deposit all or most of their energy during the rise phase of the SXR event. Thus, any model that attempts to explain all chromospheric heating in flares as due to beams must necessarily adopt an impulsive energy input with a lifetime of only a minute or so. Such an energy input mechanism cannot explain the longevity of high temperature emission in SXR events (as evidenced by Fe XXV emission, see Doschek *et al.*, 1980). All the theoretical models of SXR emission show that the temperature of the hottest part of the flare must immediately begin to decrease after cessation of the energy input (e.g., Cheng *et al.*, 1983, Pallavicini *et al.*, 1983).

Coronal heating, as evidenced by a rise in SXR emission, accompanies all flares. The same cannot be said for HXRs even in large two-ribbon flares (Dwivedi *et al.*, 1984). If beams exist in the corona, then coronal heating, either by electron beam instabilities or by Coulomb collisions, provides a more consistent explanation of SXR flare phenomena than does the beam-in-the-chromosphere model. The range of phenomena that can be explained in a consistent manner is much greater.

Arguments for beams based on the close temporal correspondence between HXR and UV emissions are considerably weakened by the recent work of Cheng and Tandberg-Hanssen (1984), who observed UV bursts (Figure 4.15) without concurrent HXR bursts. Evidently, something other than an electron beam is capable of causing flare-like bursts of transition region emission. Furthermore, the UV features that do flare simultaneously with HXR bursts begin to brighten at a time up to three minutes before HXRs are detected.

Various thermal interpretations of HXR bursts have been proposed (e.g., Brown, Melrose, and Spicer 1979), and while

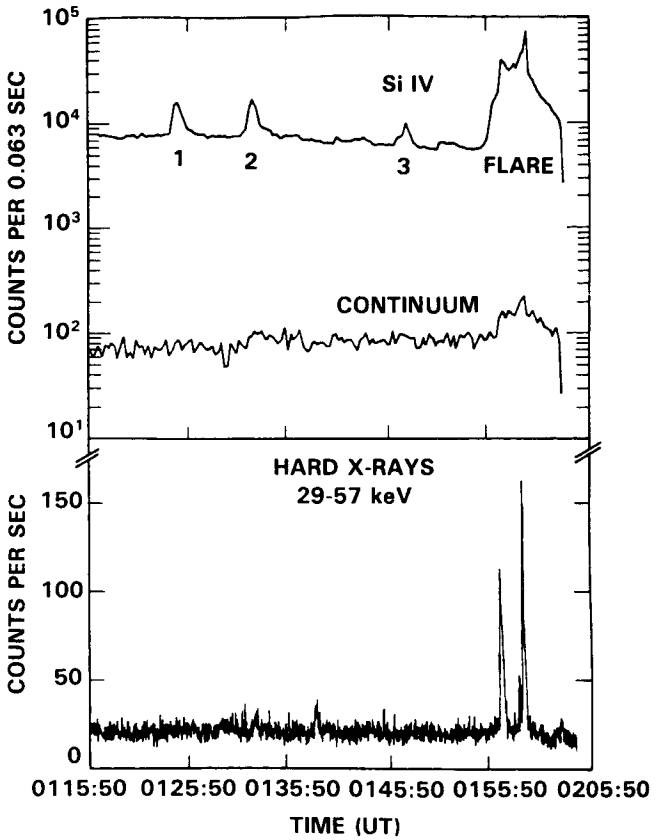

Figure 4.15 UV bursts without concurrent hard X-ray bursts (see Cheng and Tandberg-Hanssen 1984). There is also a flare in which both HXR and UV bursts occur.

a discussion of these models is outside the scope of this chapter, the impact of this alternative view of HXR bursts is important to this debate. If HXR bursts are thermal phenomena, there will be, of course, no beams in the chromosphere. Furthermore, the energy of the HXR-emitting plasma deposited in recent thermal models (Smith and Lilliquist 1979) is nearly as great as the energy deduced for electron beams from the thick-target model. Thus, the apparent agreement found for numerous flares by Antonucci (1982), and by others, between the calculated (thick-target model) electron beam energy and the SXR plasma energy shows only that a beam model offers one energetically consistent interpretation of the HXR-SXR sequence. More refined work — measurements of energy release in HXRs and SXRs for example, with high spatial and temporal resolution — will be required to distinguish between thermal and beam interpretations of coronal emission measure increases.

4.5.2.2. The Relative Importance of Conduction and Electron Beams

The temporal correspondence between UV and HXR bursts found by Woodgate *et al.* (1983) and the similar correspondence between chromospheric emissions and HXR bursts reported by Feldman, Liggett, and Zirin (1983), Zirin (1978), Rust and Hegwer (1975) and others is a persuasive argument for the presence of electron beams. However, electron beam models predict much more UV emission than is observed, so in order to rescue the electron beam interpretation of the UV-HXR correspondence, it must be supposed that the beams involved are weak. Furthermore, the ubiquity of preflare UV brightenings implies that little energy is required to produce them. Therefore, the UV-HXR correspondence does not help establish that more chromospheric evaporation is driven directly by electron beams.

Tang and Moore (1982) showed that certain chromospheric brightenings removed by $1 - 4 \times 10^5$ km from flare cores brighten simultaneously with reverse drift type III bursts, which are certainly caused by electron beams. They concluded, however, that most of the energy reaching the chromosphere at those points was not carried by the beams, but rather by conduction or shock waves, in agreement with a similar study of remote brightenings by Rust and Webb (1977). The durations of the remote brightenings greatly exceeded those of the electron beams. Yet, if attention had been focussed on onset times only, it might have been concluded that electron beams were the only heating mechanism.

Rust, Simnett, and Smith (1985) studied the flare of November 5, 1980 and showed that arrival of the electron beam was followed by arrival of thermal energy originating at the main flare site. The thermal energy, detected in 3.5 to 11 keV X-rays, propagated with a velocity of $\cong$ 1700 km s^{-1} and was interpreted as an effect of thermal conduction. The energy in the thermal wave was enough to account for the chromospheric and coronal heating at the remote flare site.

What the above-mentioned study shows is that qualitative comparisons of electron beam signatures and chromospheric brightenings are not adequate to establish that most chromospheric heating is driven by beams. Thermal conduction can deliver the bulk of the required energy to evaporate the chromosphere even if it does not arrive there quite as quickly as the (weak) electron beams whose existence is generally accepted.

Gunkler *et al.* (1984) and Canfield and Gunkler (1985) have also helped clarify the relative importance of the roles played by beams and conduction in chromospheric evaporation. They studied two flares for which they have good spatial and temporal resolution in Hα and in X-rays between 3.5 and 30 keV. Some of their data are shown in Figure 4.16, where the HXR burst profile is compared with the Ca XIX (SXR) burst profile and the Hα light curve for the flare of 1522 UT June 24, 1980. Although there is a close correspondence between the Hα peak and the HXR peak, it can be seen that Hα emission continues for 3 min after the HXR burst and that it began before it. Comparing observed and theoretical Hα profiles (Canfield, Gunkler, and Ricchiazzi

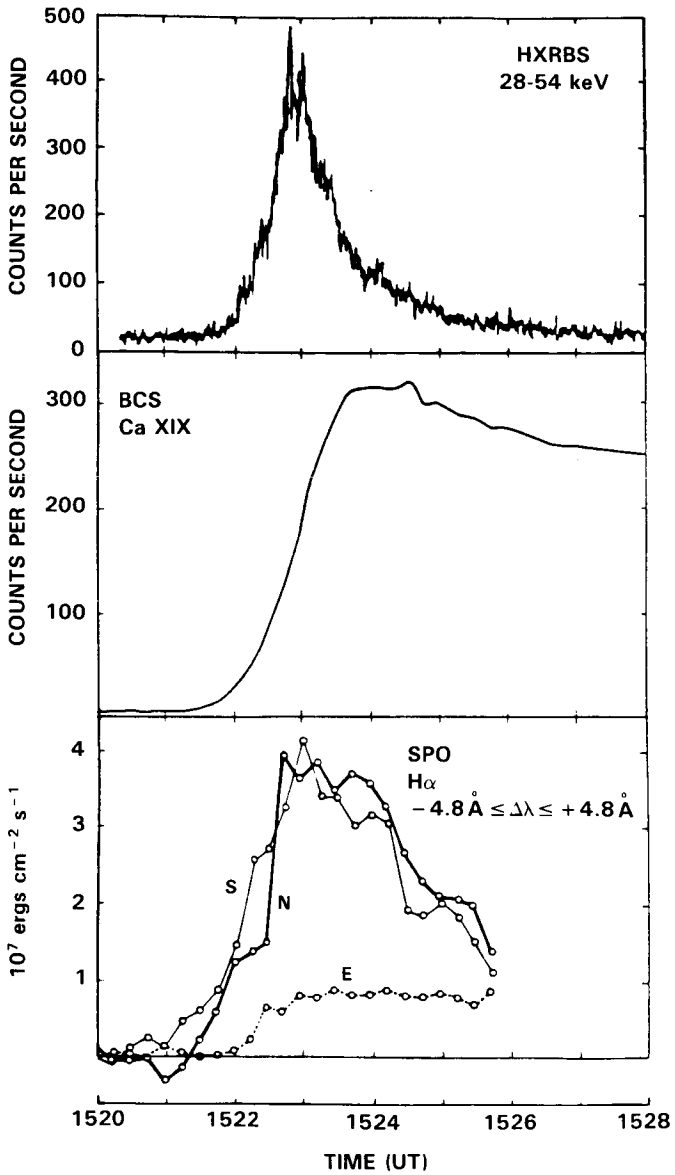

Figure 4.16 Hα data from Sacramento Peak Observatory compared with SMM BCS and HXRBS data for the June 24, 1980 flare. See text for discussion.

1984), Gunkler *et al.* (1984) concluded that nonthermal electrons were at least 2-3 times less effective than conduction in evaporating the chromosphere.

In a reanalysis (after Acton *et al.*, 1982) of the flare of 1455 UT 7 May 1980, Canfield and Gunkler (1985) find that the column depth of chromospheric plasma evaporated conductively reached 8×10^{20} cm^{-2}, whereas the inferred electron beam evaporated only 7×10^{19} cm^{-2}. Specifically, this means that the electron beam could not have raised the density in the coronal flare plasma to the observed level. They conclude that although the thick target model leads to an inferred beam energy of 3×10^{11} ergs cm^{-2} s^{-1} and although the broad wings seen in some of the Hα line profiles are consistent evidence for chromospheric heating by nonthermal electrons, it was conduction of heat to the chromosphere that produced the bulk of the SXR emitting plasma.

4.5.2.3 Simulations of Electron Beam Effects

Fisher, Canfield, and McClymont (1985a) have performed computer simulations that describe the hydrodynamic effects of chromospheric heating by electron beams. In addition, Fisher, Canfield, and McClymont (1984) found that there is an upper limit for upflows driven by chromospheric evaporation of roughly twice the sound speed of the evaporated plasma (see Section 4.5.1). For the electron energy fluxes inferred from observational limits, they found that the vertical velocities expected from his simulations ranged between 0.6 and ≈ 1 times the theoretical upper limit. However, most of the velocities during flares reported by Antonucci, Gabriel, and Dennis (1984) clustered about 0.2 and 0.25 times this limit. Thus their observations are not consistent with chromospheric evaporation by nonthermal electron beams. The calculations which best match both the observed Ca XIX temperatures and the upward velocities are those of the thermal model, with conductive fluxes not exceeding 10^{10} ergs cm^{-2} s^{-1}.

It might be supposed that the low observed velocities could be explained away with a model that takes into account the probable divergence of magnetic fields as they stretch into the corona. But, as Rabin and Moore (Workshop contribution) pointed out, the more divergent the fields are for evaporating material, the more convergent they are for precipitating electrons. An electron beam originating in the corona, therefore, will encounter magnetic mirrors higher and higher for electrons of larger and larger pitch angles. The proportion of energy lost to Coulomb collisions in the corona will increase at the expense of the proportion available to precipitating electrons.

A remark on the temperature of the material that is evaporated from the chromosphere is appropriate here. The temperature inferred from SXR observations is generally in the $10 - 20 \times 10^6$ K range, yet the only computer simulations of heating by electron beams which correspond to these temperatures (MacNeice *et al.*, 1984) require very large ($> 10^{11}$ erg cm^{-2} s^{-1}) energy input rates. This severely restricts the conditions for direct chromospheric evaporation by electron beams. If, on the other hand, evaporation is driven by conduction from a very high temperature ($3 - 10 \times 10^7$ K) plasma, there is no difficulty in establishing the observed coronal flare plasma temperatures. The conclusion is that chromospheric evaporation by beam heating does not lead to a consistent interpretation of the observations of evaporated material.

For the sake of argument, the simulations of electron beam effects in the chromosphere have been accepted as plausible, at least. The UCSD flare simulations (Fisher, Canfield, and McClymont 1985a,b,c), in particular, indicate that

chromospheric evaporation is driven by both electron beams and conduction. However, there are difficulties even in the assumption that electron beams reach the chromosphere. Analysis of density-sensitive X-ray line ratios (Doschek *et al.*, 1981) shows that the preflare coronal density is at least 2×10^{10} cm^{-3}. A substantial portion of the electron beam energy would be lost in traversing such a corona (depending on the height of the beam acceleration site), so the question of whether electrons ever penetrate the chromosphere is an open one. If a substantial part of the beam energy is lost in the corona, it would end up being thermally conducted to the chromosphere. This view is consistent with the Hα flare profile studies of Gunkler *et al.* (1984), except that they feel that there is evidence for some energetic electrons in the chromosphere where the broadest Hα line profiles are seen.

4.5.2.4 Interpretation of Hα Line Profiles

In the static flare atmospheres that have been studied to date, broad Hα line wings are produced when the electron beam ionized hydrogen at depths where the density is $\simeq 10^{14}$ cm^{-3}. It is the combination of a high degree of ionization and high pressure that produces pronounced Stark broadening in Hα. However, to be completely consistent, one should compute the Hα line profile expected from the dynamic flare atmospheres simulated by, for example, Cheng *et al.* (1983), MacNeice *et al.*, (1984), and Fisher, Canfield, and McClymont (1984). The curious feature of all these dynamic models is that a dense condensation appears in the chromosphere at a column depth of $\simeq 3 \times 10^{19}$ cm^{-2}, i.e., relatively high. Yet, the density may approach 10^{14} cm^{-3} and the pressure may be between 100 and 1000 dynes cm^{-2}. These condensations appear in model chromospheres heated by thermal conduction or by electron beams. It is left as an exercise for the reader to distinguish between the Hα line wings produced in such a condensation and those produced in the deeper layers of a chromosphere whose ionization state is enhanced by electron beam collisions.

Heating of the residual chromosphere (i.e., the chromosphere not removed by evaporation) may be accomplished either by a penetrating electron beam or by an equally penetrating flux of X-rays in the 0.1 - 10 keV range. Henoux and Nakagawa (1978) showed that X-radiation from a 10^7 K plasma can enhance the number density and temperature of electrons by factors of ten and two, respectively, just above the temperature minimum. Later, Henoux and Rust (1980) showed that a substantial portion of the Hα flux in a large two-ribbon flare could have resulted from chromospheric heating by SXR photons from the coronal flare plasma. The effect of X-ray photon heating on Hα line profiles has not yet been considered in detail, but the above-mentioned research indicates that such a study would be worthwhile in an effort to understand broad Hα line wings.

Canfield and Gunkler (1985) and Ichimoto and Kurokawa (1984) have attempted to distinguish between conduction-driven and beam-driven evaporation on the basis of asymmetries in Hα profiles. Hα profile data may eventually help to distinguish between evaporation mechanisms, but the blue asymmetries that were observed and attributed to gentle evaporation by weak beams of electrons could have been produced by the magnetically-driven motions that are common in flaring active regions. Flares are almost always associated with emerging magnetic flux and with erupting filaments. Emerging flux regions appear at flare kernels with upward velocities of $\simeq$ 10 km s^{-1}. Filaments erupt with velocities as high as 600 km s^{-1}, but velocities of 50 to 200 km s^{-1} are more common.

Red asymmetries, like blue asymmetries, can result from mass motions. The conclusion is that care must be exercised in analyzing Hα profiles without high-resolution movies, which reveal most of the magnetically-driven phenomena. For example, line asymmetries can also be produced in moving optically thick plasmas, in which case an acceleration *upwards* produces a stronger red, not blue, wing.

4.5.2.5 Conclusions

It is very difficult to make the case that most evaporation is produced directly by beams, particularly when the "evaporation" is understood to be explosive, as defined by Fisher, Canfield, and McClymont (1984). The evidence for sufficiently intense beams, even in the corona, rests on theoretical arguments that become less tenable with each new study on instabilities. If the beams do exist and if they reach the chromosphere, computer simulations show that they should produce upward velocities about three times higher than observed, if the coronal temperature is to reach observed values. On the other hand, if the beam strength is lowered to give upflows consistent with observations, then the coronal plasma is far too cool to produce the observed soft X-ray flare.

Observations of hard X-ray emission from the feet of flare loops and of simultaneous UV emission show that weak fluxes of energetic electrons do impact the chromosphere. The few quantitative studies carried out to date show, however, that only a small fraction of the observed chromospheric evaporation is affected by the beams.

Although it is possible to cast doubt on many lines of evidence for electron beams in the chromosphere, a balanced view that debaters on both sides of the question might agree to is that electron beams probably heat the low corona and upper chromosphere, but their direct impact on evaporating the chromosphere is energetically unimportant when compared to conduction. This represents a major departure from the thick-target flare models that were popular before the Workshop.

4.5.3 Recommendations for Further Research

Studies of the spatially integrated emission spectra of flares in HXRs should be deemphasized in favor of high spa-

tial and spectral resolution HXR and UV observations of preflare and flare onset behavior. Quantitative studies of UV and optical emissions at flare kernels should be conducted with the highest time resolution possible (e.g., $\simeq$ 1s), in order to separate the effects of electron beams and conduction.

The numerical simulations of chromospheric evaporation suggest that one possible manifestation of "explosive" evaporation by nonthermal electrons is the sudden appearance of high densities at coronal temperatures, and their subsequent relaxation to lower values on coronal loop hydrodynamic timescales. Some possible examples of this behavior have been found in P78-1 observations and were discussed in Section 4.5.2.3. Such observations should be carried out in future experiments with much higher time resolution (a few seconds) and with concurrent HXR observations. The numerical calculations also suggest that it might be possible to detect the threshold between gentle and explosive evaporation due to nonthermal electrons by looking for a change of sign in chromospheric velocities as the energy flux in nonthermal electrons changes from low to high values. These velocities may be detectable by looking at asymmetries in Hα profiles.

The authors would like to thank Ms. Marlene Wedding and Ms. Judy Hardison for typing the manuscript.

4.6 REFERENCES

Acton, L.W., *et al.*, 1980, *Solar Phys.*, *65*, 53.

Acton, L.W., Canfield, R.C., Gunkler, T.A., Hudson, H.S., Kiplinger, A.L., Leibacher, J.W. 1982, *Ap. J.*, *263*, 409.

Antiochos, S.K., and Sturrock, P.A. 1978, *Ap. J.*, *220*, 1137.

Antonucci, E., *et al.*, 1982, *Solar Phys.*, *78*, 107.

Antonucci, E. 1982, *Mem. Soc. Astr. Ital.*, *53*, 495.

Antonucci, E., and Dennis, B.R. 1983, *Solar Phys.*, *86*, 67.

Antonucci, E., Gabriel, A.H., Dennis, B.R. 1984, *Ap. J.*, *287*, 917.

Antonucci, E., Gabriel, A.H., Dennis, B.R., and Simnett, G.M. 1984, submitted to *Solar Phys.*

Antonucci, E., Marocchi, D., and Simnett, G.M. 1984, *Adv. Space Res.*, in press.

Brown, J.C. 1973, *Solar Phys.*, *31*, 143.

Brown, J.C., Melrose, D.B., and Spicer, D.S. 1979, *Ap. J.*, *228*, 592.

Brueckner, G.E. 1975, in Solar Gamma-, X-, and EUV Radiation (IAU Symposium No. 68), ed. S.R. Kane (Dordrecht: Reidel), p. 135.

Brueckner, G.E. 1976, *Phil. Trans. R. Soc. London A*, *281*, 443.

Canfield, R.C., and Gunkler, T.A. 1985, *288*, 353.

Canfield, R.C., Gunkler, T.A., Ricchiazzi, P.J. 1984, *Ap. J.*, *282*, 296.

Cheng, C.-C. 1977, *Solar Phys.*, *55*, 413.

Cheng, C.-C., Doschek, G.A., and Feldman, U. 1979, *Ap. J.*, *227*, 1037.

Cheng, C.-C., Feldman, U., and Doschek, G.A. 1979, *Ap. J.*, *233*, 736.

Cheng, C.-C., Karpen, J.T., and Doschek, G.A. 1984, *Ap. J.*, *286*, 787.

Cheng, C.-C., Oran, E.S., Doschek, G.A., Boris, J.P., and Mariska, J.T. 1983, *Ap. J.*, *265*, 1090.

Cheng, C.-C., and Tandberg-Hanssen, E. 1984, preprint.

Cohen, L., Feldman, U., and Doschek, G.A. 1978, *Ap. J. Suppl.*, *37*, 393.

Dere, K.P., and Cook, J.W. 1979, *Ap. J.*, *229*, 772.

Dere, K.P., and Cook, J.W. 1983, *Astr. Ap.*, *124*, 181.

Dere, K.P., Mason, H.E., Widing, K.G., and Bhatia, A.K. 1979, *Ap. J. (Suppl.)*, *40*, 341.

Deslattes, R. 1985, private communication.

Doschek, G.A. 1983, *Solar Phys.*, *86*, 9.

Doschek, G.A. 1984, *Ap. J.*, *283*, 404.

Doschek, G.A., Cheng, C.-C., Oran, E.S., Boris, J.P., and Mariska, J.T. 1983, *Ap. J.*, *265*, 1103.

Doschek, G.A., Feldman, U., and Cowan, R.D. 1981, *Ap. J.*, *245*, 315.

Doschek, G.A., Feldman, U., Dere, K.P., Sandlin, G.D., VanHoosier, M.E., Brueckner, G.E., Purcell, J.D., and Tousey, R. 1975, *Ap. J. (Letters)*, *196*, L83.

Doschek, G.A., Feldman, U., Kreplin, R.W., Cohen, L. 1980, *Ap. J.*, *239*, 725.

Doschek, G.A., Feldman, U., Landecker, P.B., McKenzie, D.L. 1981, *Ap. J.*, *249*, 372.

Doschek, G.A., Feldman, U., and Rosenberg, F.D. 1977, *Ap. J.*, *215*, 329.

Doschek, G.A., Kreplin, R.W., Feldman, U. 1979, *Ap. J. (Letters)*, *233*, L157.

Doschek, G.A., Mariska, J.T., and Feldman, U. 1981, *M.N.R.A.S.*, *195*, 107.

Duijveman, A., Hoyng, P., Machado, M.E. 1982, *Solar Phys.*, *81*, 137.

Duijveman, A., Somov, B.V., Spektor, A.R. 1983, *Solar Phys.*, *88*, *257*.

Dwivedi, B.N., Hudson, H.S., Kane, S.R., and Svestka, Z. 1984, *Solar Phys.*, *90*, 331.

Feldman, U., Cheng, C.-C., and Doschek, G.A. 1982, *Ap. J.*, *255*, 320.

Feldman, U., and Doschek, G.A. 1977, *Ap. J. (Letters)*, *216*, L119.

Feldman, U., Doschek, G.A., and Kreplin, R.W. 1982, *Ap. J.*, *260*, 885.

Feldman, U., Doschek, G.A., Kreplin, R.W., Mariska, J.T. 1980, *Ap. J.*, *241*, 1175.

Feldman, U., Doschek, G.A., and McKenzie, D.L. 1984, *Ap. J. (Letters)*, *276*, L53.

Feldman, U., Doschek, G.A., and Rosenberg, F.D. 1977, *Ap. J.*, *215*, 652.

Feldman, U., Liggett, M., and Zirin, H. 1983, *Ap. J.*, *271*, 832.

Fisher, G.H., Canfield, R.C., McClymont, A.N. 1984, *Ap. J. (Letters)*, *281*, L79.

Fisher, G.H., Canfield, R.C., McClymont, A.N. 1985a, *Ap. J.*, *289*, 414.

Fisher, G.H., Canfield, R.C., McClymont, A.N. 1985b, *Ap. J.*, *289*, 425.

Fisher, G.H., Canfield, R.C., McClymont, A.N. 1985c, *Ap. J.*, *289*, 434.

Gabriel, A.H. 1972, *M.N.R.A.S.*, *160*, 99.

Gabriel, A.H., and Jordan, C. 1975, *M.N.R.A.S.*, *173*, 397.

Grineva, U.I., *et al.*, 1973, *Solar Phys.*, *29*, 441.

Gunkler, T.A., Canfield, R.C., Acton, L.W., Kiplinger, A.L. 1984, *Ap. J.*, *285*, 835.

Henoux, J.-C., and Nakagawa, Y. 1978, *Astr. Ap.*, *66*, 385.

Henoux, J.-C., and Rust, D.M. 1980, *Astr. Ap.*, *91*, 322.

Heyvaerts, J., Priest, E.R., and Rust, D.M. 1977, *Ap. J.*, *216*, 123.

Hiei, E., and Widing, K.G. 1979, *Solar Phys.*, *61*, 407.

Hoyng, P., *et al.*, 1981, *Ap. J.*, *246*, L155.

Hudson, H. 1983, private communication.

Ichimoto K., and Kurokawa, K. 1984, *Solar Phys.*, submitted.

Jordan, C. 1975, private communication.

Jordan, C. 1985, submitted to *Solar Phys.*

Kane, S.R., Fenimore, E.E., Klebesadel, R.W., and Laros, J.G. 1982, *Ap. J. (Letters)*, *254*, L53.

Korneev, V.V., Zhitnik, I.A., Mandelstam, S.L., Urnov, A.M. 1980, *Solar Phys.*, *68*, 391.

Kostyuk, N.D., and Pikel'ner, S.R. 1975, *Sov. Astron.*, *18*, 590.

Kostyuk, N.D. 1976, *Sov. Astron.*, *20*, 206.

Kreplin, R.W., Doschek, G.A., Feldman, U., Seely, J.F., and Sheeley, N.R., Jr. 1985, *Ap. J.*, in press.

Lin, R.P., and Hudson, H.S. 1976, *Solar Phys.*, *50*, 153.

Livshits, M.A., Badalyan, O.G., Kosovichev, A.G., Katsova, M.M. 1981, *Solar Phys.*, *73*, 269.

MacNeice, P., McWhirter, R.W.P., Spicer, D.S., and Burgess, A. 1984, *Solar Phys.*, *90*, 357.

Martin, S.F., and Ramsey, H.E. 1972, in *Solar Activity, Observations and Predictions*, ed. P.S. McIntosh and M. Dryer (Cambridge: MIT Press), p. 371.

Mason, H.E., Shine, R.A., Gurman, J.B., and Harrison, R.A., 1985, preprint.

McClymont, A.N., Canfield, R.C., Fisher, G.H. 1985, in preparation.

Moore, R.L., *et al.*, 1980, in *Solar Flares*, ed. P.A. Sturrock (Boulder: Colorado Associated University Press), p. 341.
Moore, R.L., Hurford, G.J., Jones, H.P., and Kane, S.R. 1984, *Ap. J., 276*, 379.
Moore, R.L., and Kahler, S. 1984, in preparation.
Nagai, F. 1980, *Solar Phys., 68*, 351.
Nagai, F., and Emslie, G. 1983, preprint.
Pallavicini, R., Serio, S., and Vaiana, G.S. 1977, *Ap. J., 216*, 108.
Pallavicini, R., Peres, G., Serio, S., Vaiana, G., Acton, L., Leibacher, J., and Rosner, R. 1983, *Ap. J., 270*, 270.
Ricchiazzi, P.J., and Canfield, R.C. 1983, *Ap. J., 272*, 739.
Rust, D.M., and Hegwer, F. 1975, *Solar Phys., 40*, 141.
Rust, D.M., Simnett, G.F., and Smith, D.F. 1985, *Ap. J., 288*, 401.
Rust, D.M., and Webb, D.G. 1977, *Solar Phys., 54*, 403.
Smith, D.F., and Lilliequist, C.G. 1979, *Ap. J., 232*, 582.
Somov, B.V., Syrovatskii, S.I., Spektor, A.R. 1981, *Solar Phys., 73*, 145.
Somov, B.V., Sermulina, B.J., Spektor, A.R. 1982, *Solar Phys., 81*, 281.
Svestka, Z. 1976, *Solar Flares*, D. Reidel Publ. Co., Dordrecht, Holland.
Tanaka, K., Watanabe, T., Nishi, K., Akita, K. 1982a, *Ap. J. (Letters), 254*, L59.
Tanaka, K., Akita, K., Watanabe, T., Nishi, K. 1982b, Hinotori Symposium on Solar Flares, Tokyo, 43.
Tanaka, K., Ohki, K., and Zirin, H. 1985, preprint.
Tanaka, K. 1984, presentation at the 3rd SMM Workshop.
Tang, F., and Moore, R.L. 1982, *Solar Phys., 77*, 263.
Van Beek, H.F., Hoyng, P., Lafleur, B., Simnett, G.M. 1980, *Solar Phys., 65*, 39.
Widing, K.G. 1975, in *Solar Gamma-, X-, and EUV Radiation*, page 153, proceedings of IAU Symposium No. 68, edited by S.R. Kane (D. Reidel Publ. Co., Dordrecht, Holland).
Widing, K.G., and Dere, K.P. 1977, *Solar Phys., 55*, 431.
Widing, K.G., and Hiei, E. 1984, *Ap. J., 281*, 426.
Woodgate, B.E., Shine, R.A., Poland, A.I., Orwig, L.E. 1983, *Ap. J., 265*, 530.
Zirin, H. 1978, *Solar Phys., 58*, 95.